Chapter 4

Optical Frequency Combs for Molecular Spectroscopy, Kinetics, and Sensing

Julia H. Lehman*,[1] and Marissa L. Weichman*,[2]

[1]School of Chemistry, University of Leeds, Leeds LS2 9JT, United Kingdom

[2]Department of Chemistry, Princeton University, Princeton, New Jersey 08544, United States

***Email: j.lehman@leeds.ac.uk.**

***Email: weichman@princeton.edu.**

Downloaded via PRINCETON UNIV on May 9, 2024 at 15:15:05 (UTC).
See https://pubs.acs.org/sharingguidelines for options on how to legitimately share published articles.

With rapidly developing technological advances and increasing commercialization, optical frequency combs are beginning to see use in chemical laboratories around the world. These light sources allow chemists to collect high-resolution, multiplexed direct absorption spectra in a fraction of the laboratory time required by more conventional methods. Broadband coupling of combs into high-finesse optical cavities continues to break new ground in the sensitivity of both frequency- and time-resolved spectroscopies. Analytical sensing applications are also undergoing a burst of activity as comb systems become miniaturized, turn-key, and more robust in rugged environments. In this Chapter, we introduce frequency comb spectroscopy and survey its recent applications to molecular spectroscopy and dynamics, chemical reaction kinetics, and sensing.

1. Introduction

Optical frequency combs, laser light sources whose frequency-domain spectra consist of a series of narrow evenly spaced lines, have become a robust tool in the arsenal of techniques available to modern physical and analytical chemists. Frequency combs were initially developed through a fruitful marriage of the fields of ultrafast science and precision measurement (*1*, *2*) and enabled direct referencing between radiofrequency (RF) and optical standards. They subsequently revolutionized atomic physics and metrology. The use of frequency combs as an attractive light source for chemistry has been realized more recently, and their applications to major problems in molecular spectroscopy, chemical kinetics, and sensing are beginning to be borne out. In this Chapter, we highlight emerging techniques using frequency combs that have already enabled new chemical science or that show significant promise in the near future. We give brief context here for some technical aspects of working with comb sources, and also refer the reader to previous comprehensive reviews of the development and evolution of frequency comb technology (*3*–*6*), its particular uses for direct

© 2021 American Chemical Society
Berman et al.; Emerging Trends in Chemical Applications of Lasers
ACS Symposium Series; American Chemical Society: Washington, DC, 2021.

spectroscopy and sensing (*7*–*9*), and comparisons between frequency comb systems and other technologies (*9*, *10*).

The optical frequency comb is a simultaneously broadband and precise light source. It can be thought of as a single laser oscillator emitting thousands of narrow-linewidth continuous-wave (cw) laser lines in parallel, each with well-defined frequency and phase relationships to its neighbors. This unusual light source is the foundation for frequency comb spectroscopy (FCS), a nearly ideal method for kinetics and sensing which (a) is broadband, allowing multiplexed detection of various species and spectral features simultaneously; (b) has excellent frequency resolution, allowing full analysis and identification of the states and species detected; (c) allows high signal-to-noise measurements, to detect trace species or weak features; and (d) has the potential for fast readout, for flexibility of use and to follow chemistry in real time. FCS can meet all of these challenging criteria, often in one experiment. Ongoing technical developments are pushing the capabilities of comb systems to meet these demands, and optimizing their size, simplicity, and ruggedness when deployed in the field.

Most frequency combs, though not all, are generated via stabilization of an ultrafast mode-locked laser. In the time domain, a mode-locked laser emits a train of pulses spaced with time period τ or, equivalently, repetition rate f_{rep} (Figure 1). A Fourier transform of this time domain picture to the frequency domain yields a spectrum of discrete optical features, so-called "comb teeth," evenly spaced by the laser repetition rate. The comb teeth have frequencies ν_m given by

$$\nu_m = m \cdot f_{rep} + f_0 \tag{1}$$

where m is an integer and f_0 is a fixed offset frequency common to all teeth. These ν_m correspond to the frequencies of longitudinal modes of the laser oscillator cavity, whose relative phases are constrained by mode-locking to enforce the formation of ultrafast pulses. The f_0 offset, often called the carrier-envelope offset frequency, derives from dispersion within the laser oscillator cavity which causes a pulse-to-pulse phase slip $\Delta\varphi_{CE}$ of the oscillating carrier wave with respect to the pulse envelope.

Provided that f_{rep} and f_0 are measured and stabilized, these two radiofrequencies constrain the position of every comb tooth and yield a well-determined optical spectrum. It is this feature that allows frequency combs to link RF and optical standards and to serve as a powerful tool for metrology and precision spectroscopy. Determining f_{rep} and f_0 is therefore critical to the practical use of frequency combs. Because the intensity of the electric field emitted by a mode locked laser is modulated by f_{rep}, f_{rep} can be accessed simply by measuring the laser output on a photodetector and beating this signal against an RF reference. The measurement of f_0 is more subtle, as the oscillations of the carrier wave are too fast to detect directly. f_0 frequencies are typically measured by self-referenced f-$2f$ interferometry, wherein a comb is split into two arms, frequency doubled in one arm and broadened in nonlinear fiber in the other to span more than an octave. Beating the $2\nu_n$ comb lines against the nearest ν_m line yields an RF signal at f_0. The implementation of this interferometry scheme was a historical challenge hindering comb stabilization, until technological breakthroughs in nonlinear fiber development permitted the generation of octave-spanning combs (*11*, *12*). f_0 can also be passively cancelled, as is possible for combs derived from difference frequency generation, whose spectra therefore consist solely of integer multiples of f_{rep} (*13*).

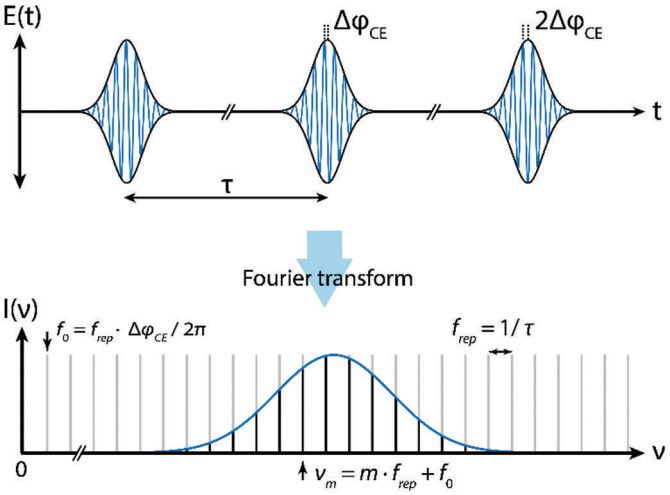


Figure 1. The time domain representation of a mode-locked ultrafast laser pulse train and the corresponding frequency domain representation demonstrating the formation of comb teeth. Reproduced with permission from reference (8). Copyright 2019 Elsevier.

In this Chapter, we emphasize the applications of both stabilized and free-running combs for direct spectroscopy. In direct FCS, comb light is sent through a molecular sample and its spectrum is subsequently recorded, often with resolution of the attenuation of individual comb teeth due to sample absorption. Several laser platforms permit the generation of optical frequency combs relevant to molecular spectroscopy and sensing (Figure 2a), spanning wavelengths from the terahertz (THz) to the extreme ultraviolet (XUV). Direct FCS has now been applied in a variety of sample configurations, including flow cells, high-finesse optical cavities, and open paths in the field (Figure 2b). Various platforms for spectral readout with comb-mode resolution are compatible with these measurements, each with its tradeoffs in acquisition speed, bandwidth, and apparatus complexity (Figure 2c). We now briefly review these relevant experimental components.

While the initial demonstrations of frequency combs based on mode-locked lasers were carried out with solid state Ti:Sapphire systems, fiber-based systems are now the most commonly adopted comb technology. The gain medium of a fiber comb oscillator is a glass fiber doped with rare earth metal cations lasing in the near-infrared (IR), most commonly erbium, ytterbium, or thulium. Fiber lasers have been widely adopted due to a combination of convenient properties: they are robust, relatively inexpensive, and feature high achievable powers and broad gain bandwidth (*14*). Various methods of frequency conversion have been used to extend the native near-IR frequencies of fiber combs to more useful spectral windows. Fiber comb light can be broadened in highly nonlinear fiber to generate a near-IR supercontinuum (*15*). Difference frequency generation and optical parametric oscillation in nonlinear crystals have enabled broadband, tunable comb sources spanning visible and mid-IR wavelengths (*16*–*23*). Production of coherent combs in the XUV has been achieved through high harmonic generation carried out in a resonant optical cavity (*24*).

In recent years, much work has been done to enable novel comb sources that are more compact and frequency agile than mode-locked lasers (*5*, *6*). Microresonator combs, or microcombs, can be synthesized by coupling a cw laser into a high-quality factor whispering gallery mode resonator or ring resonator where light is confined by total internal reflection. The strong nonlinearities in the resonator material result in four-wave-mixing processes that generate cascaded sidebands on the cw carrier and can form mode-locked soliton pulses (*25*, *26*). Complete self-referencing (*27*) and

dual comb spectroscopy (DCS) (*28*) have recently been demonstrated with microcombs, and there are exciting possibilities for their chip-scale applications. A related development are electro-optic (EO) combs, wherein cascaded sidebands are placed on a cw carrier using EO modulation (*29*). In principle, EO combs can be extremely frequency agile, making use of a tunable cw pump laser and a digitally programmable repetition rate. A fully referenced, octave-spanning EO comb has now been demonstrated, though the implementation is technically challenging (*30*). The development of quantum cascade laser and interband cascade laser frequency combs is also notable, as these semiconductor lasers are the only currently available comb sources that emit directly in the mid-IR and offer electrical rather than optical pumping (*31*, *32*). While these systems do not produce ultrafast pulses and have not yet been self-referenced, they show significant promise for free-running mid-IR DCS (*33*, *34*).

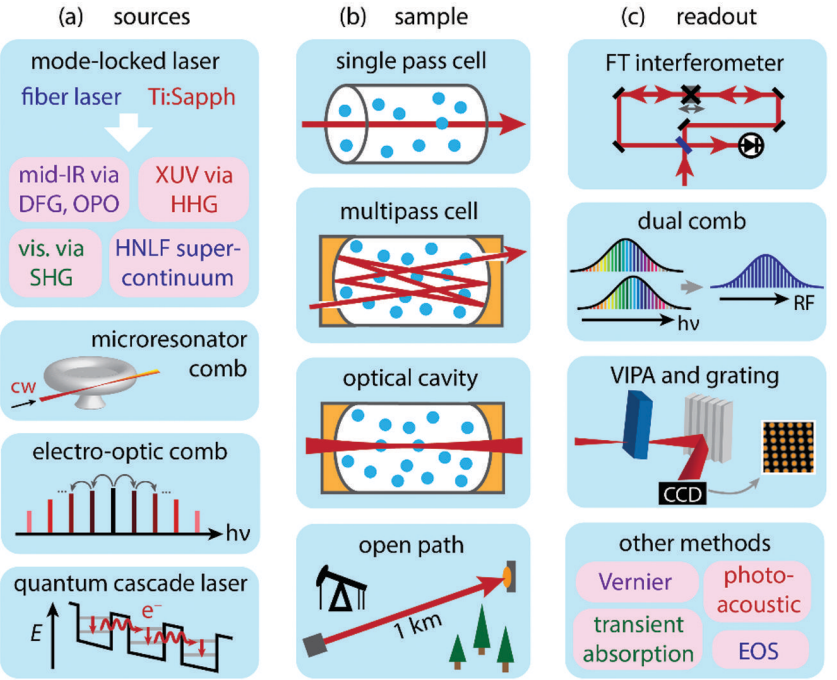


Figure 2. An overview of common (a) frequency comb sources, (b) sample geometries, and (c) spectral readout methods harnessed for molecular spectroscopy, kinetics, and sensing. Abbreviations: DFG, difference frequency generation; OPO, optical parametric oscillator; XUV, extreme ultraviolet; HHG, high harmonic generation; SHG, second harmonic generation; HNLF, highly nonlinear fiber; FT, Fourier transform; VIPA, virtually imaged phased array; EOS, electro-optical sampling.

Combs have been applied to molecular samples in a variety of configurations, some of which are summarized in Figure 2b. Beyond simple single-pass transmission measurements, multipass cells and optical cavities offer significantly improved measurement sensitivity through pathlength enhancement. In particular, the longitudinal mode structure of an optical cavity is a beautiful match for the regularly spaced teeth of a frequency comb, allowing the comb light to be resonantly coupled to the cavity over a broad spectral window (*7*, *35*, *36*). Open path trajectories are also commonly used for increased sensitivity in comb-based sensing. These configurations will be discussed in the case studies detailed later in this Chapter.

Several methods are widely used to resolve comb spectra following transmission through a sample. Comb-mode resolution is commonly achieved via interferometric readout methods. Fourier transform (FT) interferometry, as used in commercial broadband FT spectrometers, is perhaps the most general method, wherein a scanning delay stage is used to self-interfere comb light to generate an interferogram (*37*–*39*). The major shortcomings of this technique are the need for mechanical moving parts and correspondingly long acquisition times. DCS is an alternative interferometric method wherein the scanning arm is replaced by a second comb of slightly different repetition rate, $f_{rep} + \Delta f_{rep}$, beat against the first comb on a photodetector to yield an interferogram with repetition rate Δf_{rep} (*40*). DCS allows for rapid, broadband, comb-mode resolved measurements but generally requires two separate combs that are mutually coherent. DCS methods are coming to the fore as comb sources become cheaper and more compact. The use of two EO combs originating from a single cw laser can dramatically reduce DCS apparatus complexity due to high mutual coherence (*41*, *42*). Recent work has also pushed to produce dual combs from single laser oscillators (*43*–*46*), and to enable computational coherent averaging techniques to compensate for the spectral instabilities of free running combs (*47*–*51*).

A distinct approach to comb-mode resolution involves spatially dispersing comb light onto a detector array, best demonstrated with virtually imaged phased array (VIPA) etalons (*35*, *52*) or immersion gratings (*53*) which display very high angular dispersion. A second orthogonal dispersive optical element separates overlapping VIPA mode orders to create a two-dimensional image. The resulting spectrum can be read out with comb-mode resolution (*54*, *55*) and better than 10 μs time resolution, making VIPA-based comb spectrometers a powerful tool for chemical kinetics and the detection of transient molecular species (*53*, *55*–*58*). While the interferometric and dispersive detection methods already mentioned have facilitated the bulk of comb spectroscopies relevant for chemistry, a plethora of other methods have been demonstrated and are worth brief mention here, including electro-optic sampling of THz and mid-IR comb pulses (*59*, *60*). Vernier spectroscopy (*61*, *62*), broadband photoacoustic spectroscopy (*63*–*65*), cavity-enhanced ultrafast transient absorption (*66*), Ramsey comb spectroscopy (*67*), and comb-based quantum logic spectroscopy (*68*, *69*). Some of these developments will be discussed in further detail later on in this Chapter.

Regardless of detection scheme, if individual comb lines are resolved, the recorded spectrum will be precisely sampled at the native comb tooth spacing f_{rep}. f_{rep} is typically a radiofrequency in the vicinity of a few 100 MHz for mode locked lasers, but can reach 10-100 GHz for combs based on microresonator or semiconductor laser architectures. Combs with high repetition rates are useful for DCS, enabling fast acquisition times, and can also be fully mode-resolved with VIPA spectrometers. On the other hand, the more densely sampled spectrum of a lower repetition rate comb is often more appropriate for high-resolution spectroscopy, and comb-mode resolution remains possible with an FT interferometer or DCS. Comb light can also be filtered by locking to an optical cavity with a free spectral range incommensurate with f_{rep} to effectively increase the repetition rate of the transmitted light (*70*). When sampling at f_{rep} is too sparse to capture narrow molecular features, comb spectra acquired with discretely stepped f_{rep} or f_0 can be interleaved. The frequency resolution of a spectrum constructed in this fashion is ultimately limited by the comb tooth linewidth.

In the following sections we discuss applications of combs to important problems in molecular spectroscopy, chemical kinetics, and sensing, with a focus on recent case studies of particular interest. We conclude with our outlook on the future of comb methods as the technology matures and becomes more widely adopted.

2. Applications

2.1. Molecular Spectroscopy and Dynamics

The benefits afforded by the use of frequency combs as light sources for spectroscopy have enabled enormous breakthroughs in measurements of fundamental molecular structure and dynamics. Combs have now been integrated into a variety of cutting-edge spectroscopic infrastructures yielding drastic improvements in precision, bandwidth, sensitivity, and readout times. Here we place emphasis on work harnessing combs as light sources for direct spectroscopy, though it is important to note that combs have widespread and critical applications in frequency referencing and stabilization of cw experiments. We discuss four frontier case studies in molecular frequency comb spectroscopy, emphasizing state-resolved spectroscopy of large molecules, gas-phase ultrafast transient absorption, precision studies of molecular ions, and broadband sub-Doppler spectroscopy.

2.1.1. Cavity-Enhanced Direct Comb Spectroscopy of Large Molecules

High-resolution spectroscopy is a powerful tool to reveal the rich internal structure of small molecules in their electronic, vibrational, rotational, and spin degrees of freedom. Achieving a similarly detailed, state-resolved picture of increasingly large molecules is an important frontier, but is subject to stringent experimental requirements. Large molecules have correspondingly large densities of vibrational states, making internal cooling essential to avoid spectral congestion from hot bands. Intramolecular vibrational relaxation (IVR) can cause intrinsic spectral congestion even at relatively low internal energies. A large moment of inertia also leads to very dense rotational structure and demands high spectral resolution.

Mid-IR cavity-enhanced frequency comb spectroscopy (CE-FCS) applied to cryogenically-cooled molecular samples is a promising combination of methods by which to pursue rovibrational spectroscopy of increasingly large species (Figure 3a) (*71*, *72*). CE-FCS (*7*, *36*) is a method of direct FCS wherein the broadband spectrum of comb teeth is resonantly coupled into a series of longitudinal modes of a high-finesse optical cavity surrounding the absorber of interest. Cavity enhancement dramatically improves the sensitivity of absorption measurements via pathlength enhancement while retaining the other advantages of direct FCS (*73*). Making these absorption measurements in the mid-IR is also critical for studies of large species. In the mid-IR, vibrational fundamental transitions and low-frequency modes are accessible, Doppler broadening is reduced, and low internal energies help avoid congestion from IVR. Cooling the molecules of interest through collisions with an inert buffer gas inside a cryogenic buffer gas cell (CBGC) is a nearly universal means to build significant population in the vibrational ground state and enables the measurement of meaningful structure without obfuscation from hot populations (*71*, *72*).

A new record in rovibrational quantum state resolution of large molecules was reported by Changala *et al.* in a CE-FCS study of the C_{60} fullerene (*74*). C_{60} is an attractive spectroscopic target due to its rare icosahedral symmetry and importance in astrochemistry. The authors cooled an ensemble of C_{60} molecules in an intracavity CBGC, quenching vibrational hot bands and thermalizing the sample to a rotational temperature of 150 K. The sample was interrogated with a mid-IR DFG comb near 8.5 μm which was spectrally resolved with a scanning arm FT interferometer. A 50 cm^{-1} bandwidth of comb light was simultaneously cavity-coupled and the comb teeth stabilized to 50 kHz linewidths. f_{rep} was stepped to sample the spectrum with a spacing of

3 MHz. Data was acquired for ~20 hours, ultimately reaching a noise floor of 0.2 ppm fractional absorption per pass through the cavity, in line with earlier reported sensitivity for this apparatus (*72*).

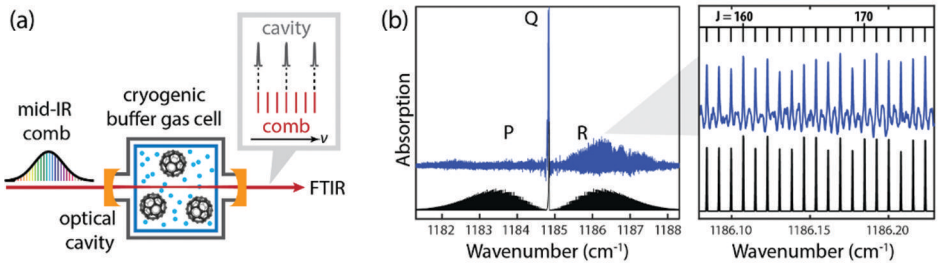


Figure 3. (a) Schematic of a cavity-enhanced frequency comb spectrometer coupled to a cryogenic buffer gas cell containing the absorber of interest. The evenly spaced comb teeth are resonantly coupled into the longitudinal modes of a high-finesse optical cavity. (b) The experimental rovibrational spectrum of cold C_{60} (blue) is plotted against a spherical top simulation fit to the experimental data (black). The cold spectrum exhibits P, Q, and R branches; the R branch in particular (inset) features sharp, well-resolved rovibrational transitions. Figure 3 adapted with permission from reference (74). Copyright 2019 The American Association for the Advancement of Science.

The resulting CE-FCS spectrum reveals a rotationally-resolved vibrational band of C_{60} (Figure 3b). Over 300 R branch transitions were observed and assigned according to their total angular momentum quantum number *J*. These spectral lines are spaced by ~240 MHz and demonstrate 15-30 MHz linewidths governed by a convolution of Doppler and pressure broadening. CE-FCS proved particularly well-suited to resolve the spectrally dense and narrow structure of these features. The R branch transition frequencies were modeled and interpreted with a rovibrational spherical top simulation allowing extraction of extremely precise rovibrational spectroscopic constants of C_{60} for the first time. The combination of CE-FCS and buffer gas cooling is clearly an apt tool for pushing the boundaries of the size and complexity of molecular systems that can be interrogated with complete quantum state resolution, with potential to probe more exotic fullerenes, radicals, and clusters in future work.

2.1.2. Cavity-Enhanced Ultrafast Transient Absorption

Broadband cavity-enhancement of frequency combs is powerful for time-resolved spectroscopy in addition to high frequency resolution measurements. Ultrafast spectroscopy gives access to important dynamical information in the time domain, particularly in complex systems where the frequency-domain picture is unresolved or too congested to be interpretable. Ultrafast transient absorption (TA) signals are routinely measured in condensed-phase samples (*75*), but extending this characterization method to dilute gas-phase samples has been an ongoing challenge due to the demanding sensitivity required. While gas-phase ultrafast dynamics are accessible with time-resolved photoelectron-based action spectroscopies, these measurements probe final states and observables that are very different from those of the corresponding solution-phase measurements. Broadband, all-optical TA of dilute gas-phase molecules would provide direct comparison between ultrafast condensed- and gas-phase measurements made with the same observables.

In 2016, Reber *et al.* reported a novel scheme for pump-probe spectroscopy in a low-density molecular beam using cavity-enhanced frequency combs (*66*). The authors harnessed the fact that mode-locked fiber combs supply femtosecond pulses suitable for ultrafast spectroscopy while

maintaining discrete teeth that can be resonantly coupled to optical cavities. Reber *et al.* locked pump and probe combs centered at 529 nm to two bow-tie cavities which were spatially overlapped at the molecular beam sample. The resulting enhancement in TA signal is proportional to the product of the pump and probe cavity finesses. The authors observed vibrational beating on the excited state surface of I_2 with a demonstrated ΔOD of 1×10^{-9} $Hz^{-1/2}$, three orders of magnitude more sensitive than any previous demonstration (*76*). However, this demonstration was made at a single probe frequency of 529 nm with no resolution of the comb spectrum. Expanding this technique to acquire a broadband gas-phase optical spectrum required the development of considerable additional infrastructure, including dispersion-managed broadband optical cavities (*77*) and an optical parametric oscillator (OPO) to generate a broadly tunable visible comb (*22*).

Silfies *et al*. (*78*) have now incorporated these developments and reported a fully broadband implementation of cavity-enhanced ultrafast TA, using a 355 nm pump pulse to initiate photochemistry and an OPO probe pulse tunable over the entire visible range from 450-700 nm. The probe comb was coupled into a bow-tie enhancement cavity whose mirrors were designed for minimal group delay dispersion over a wide spectral range. Probe comb pulses with center frequencies spanning the entire visible range can therefore be resonantly coupled with relatively high finesse. The probe cavity maintains the time resolution of comb pulses so that ultrafast TA measurements can be made with a time resolution of ~200 fs. As the simultaneous intracavity bandwidth was limited to ~10 THz, the probe comb's central frequency was scanned in order to construct a broadband spectrum. The authors reported TA of two jet-cooled molecules, 1′-hydroxy-2′-acetonaphthone and salicylideneaniline, prototypical systems for excited state intramolecular proton transfer. In both systems, Silfies *et al.* measured time constants in line with prior solution-phase measurements but in significant contrast with those measured with time-resolved photoelectron spectroscopies. These results highlight the importance of ultrasensitive, all-optical ultrafast measurements for bridging gas-phase, solution-phase and theoretical work. Additionally, while multidimensional comb spectroscopy has been reported for atomic systems (*79*, *80*), it has not yet been demonstrated with molecules or in combination with cavity enhancement. The work of Silfies, Reber, and coworkers could enable the extension of nonlinear methods like two-dimensional IR spectroscopy to dilute gas-phase samples (*81*), which currently have no action spectroscopy analogs.

2.1.3. Frequency Combs for Precision Spectroscopy of Small Molecules and Ions

Molecular ions are a rich class of species for which precision spectroscopic interrogation has long been a tantalizing target and an experimental challenge. Rotational and vibrational spectroscopy of ions is critical to their identification in astrochemical environments, where rapid, barrierless ion-molecule reactions are believed to drive molecular complexity (*82*, *83*). In atomic, molecular, and optical physics, precision spectroscopy of molecular ions enables their utility for studies of ultracold chemistry (*84*), tests of fundamental physics beyond the standard model (*85*), and platforms for quantum information and computing (*86*). Due to their daunting syntheses, extreme reactivity, and low achievable number densities, molecular ions are difficult to prepare and probe in the laboratory.

Action spectroscopies and velocity modulation spectroscopy (VMS) have come to the fore for sensitive state-resolved spectroscopy of molecular ions. The integration of optical frequency combs for referencing and readout have dramatically enhanced the precision of these measurements. In most ion action spectroscopies, ions are excited with scanned cw laser radiation and the effects of resonant absorption are monitored via resulting changes to the mass spectrum. Absolute referencing of the

cw laser frequency to a comb has enabled measurements with sub-MHz resolution (*87*), including studies of benchmark astrochemical systems like the H_3^+ cation (*88*), and extremely challenging targets like the fluxional CH_5^+ cation (*89*). VMS is a complementary technique wherein the electric field of the ion discharge source is modulated, causing an oscillating Doppler shift of ion absorption features that can be detected with a lock-in amplifier. VMS techniques are almost always used with absolute frequency comb referencing of the cw laser light to achieve spectral uncertainties on the few-MHz level (*90*). Cavity-enhanced VMS has also been successfully implemented with a broadband comb as the direct light source (*91*, *92*).

A recent development in comb-based ion spectroscopy is the work of Chou *et al.* to interrogate the THz rotational transitions of a single molecular ion using frequency comb Raman spectroscopy and quantum logic techniques (*69*). A single $^{40}CaH^+$ ion was co-trapped in an ion trap with a laser cooled $^{40}Ca^+$ ion. The quantum state of $^{40}CaH^+$ was first prepared using quantum logic spectroscopy (*86*). The authors then coherently drove stimulated THz Raman rotational transitions in $^{40}CaH^+$ using two arms of a stabilized Ti:Sapph frequency comb. The probability that the Raman transition occurred was measured using quantum logic spectroscopy as the comb tooth frequencies were scanned. Rotational transition frequencies were reported with uncertainties at the kHz level, limited by the coherence of the stabilized comb, which could be improved to the Hz level or better in future work. This technique can also be adapted to Raman measurements of IR, rather than THz, transitions by using increasingly broadband combs. Since the Raman comb laser is detuned from resonance, it is not specific to this molecular system and can in principle be harnessed for studies of more complex polyatomic ions of chemical interest.

2.1.4. Broadband Sub-Doppler Spectroscopy with Frequency Combs

Frequency combs are continually being integrated in novel experimental configurations for broadband precision spectroscopy. Doppler broadening due to the thermal distribution of velocities in an ensemble of absorbers is often the limiting factor in the spectral linewidths of gas-phase species, presenting an intrinsic constraint for high-resolution measurements. Sub-Doppler spectroscopies make use of intense illumination with a spectrally narrow pump laser to transfer a significant fraction of a specific velocity class of molecules from one state to another. The resulting spectral signatures are governed by homogeneous broadening processes rather than Doppler broadening. Observation of these sub-Doppler signatures can be critical not only for precision measurements, but for disentangling congested spectra where state splittings fall within the Doppler linewidth. However, sub-Doppler measurements remain typically limited by the accuracies and tuning ranges of the lasers involved. Foltynowicz *et al.* recently reported a sub-Doppler double resonance spectroscopy (DRS) scheme using a frequency comb as a broadband probe (*93*, *94*). The authors applied this apparatus to study the vibrational overtones of the ν_3 mode of methane (CH_4). Spectral data on highly vibrationally-excited states of CH_4 are important for benchmarking theoretical predictions of high-temperature spectra, with intriguing applications for spectroscopy of exoplanet atmospheres (*95*). While comb-referenced DRS methods have been used previously to great effect (*96–98*), and sub-Doppler comb spectroscopy has been reported for atomic systems (*99*), this work represents the first sub-Doppler work using direct FCS on any molecular system.

DRS is a common implementation of sub-Doppler spectroscopy. A narrow linewidth pump laser saturates a specific rovibrational transition, and a probe laser measures depletion features in transitions that share a common lower state with the pumped transition (V type transitions) or the

appearance of new excited state absorption features (ladder transitions), as shown in Figure 4a and 4b for both cw and comb probes. Foltynowicz *et al.* used a Lamb dip lock to stabilize a cw pump laser to a series of nine distinct rovibrational lines of CH_4 near 3.3 μm. The comb probe near 1.67 μm allowed for simultaneous detection of more than 10,000 spectral elements over a 200 cm^{-1} bandwidth, detected via scanning arm FT interferometer with comb mode resolution and a noise equivalent absorption coefficient of 7.2×10^{-6} cm^{-1} after 3.2 hours of averaging. The probe comb f_{rep} was scanned to sample the spectrum with 2 MHz steps.

The combination of wide spectral coverage and high frequency accuracy of Foltynowicz and coworkers' probe comb enabled the detection of 18 sub-Doppler V-type rovibrational transitions between the vibrational ground state and the $2\nu_3$ band (Figure 4c) and 36 novel $3\nu_3 \leftarrow \nu_3$ ladder-type transitions. The authors reported orders-of-magnitude better frequency precision than prior spectroscopic studies of the $3\nu_3$ manifold of CH_4 (*100*). The ultimate frequency accuracy of these measurements remains limited to ~1 MHz by the stabilization of the cw pump laser. Stabilizing the cw pump laser via frequency comb referencing could ultimately improve the resolution to the kHz level (*97*, *98*). The addition of an enhancement cavity for the broadband comb probe could improve sensitivity and enable the extension of these measurements to more challenging spectroscopic targets that cannot be prepared in high concentration.

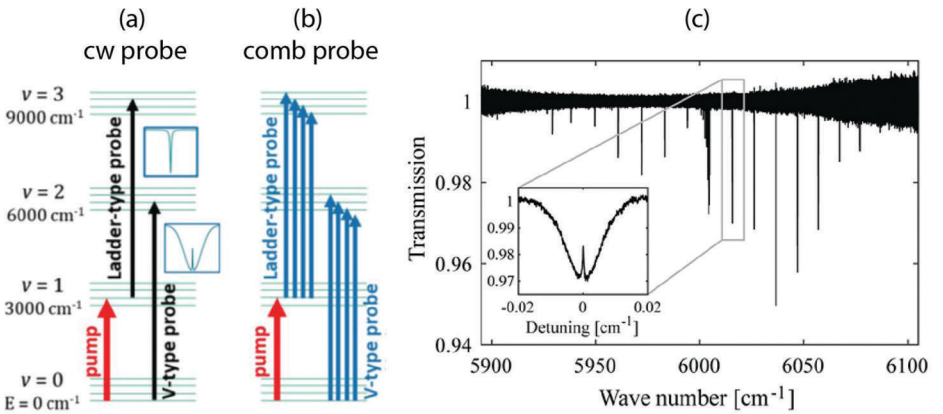


Figure 4. V-type and ladder-type double resonance transitions studied in the ν_3 overtone transitions of methane with a (a) cw or (b) frequency comb probe. (c) Comb probe spectrum of methane near 6000 cm^{-1} acquired with the pump laser on resonance with the ν_3 fundamental R(0) transition, showing a subsequent V-type probe transition in the $2\nu_3$ overtone R(0) transition. Figure 4 adapted with permission from reference (93). Copyright Foltynowicz et al., some rights reserved; exclusive licensee American Physical Society. Distributed under a Creative Commons Attribution License 4.0 (CC BY) https://creativecommons.org/licenses/by/4.0/.

2.2. Chemical Reaction Kinetics

A natural application of FCS is the measurement of spectra of reacting mixtures as a function of time, akin to *in situ operando* spectroscopy used in the field of catalysis (*101*) Understanding reaction kinetics is fundamental to all areas of chemistry, ranging from fuel combustion to protein folding dynamics (*102*). The quantitative determination of reaction rate coefficients and product branching

ratios yields insight into reaction mechanisms, which can, in turn, enable prediction and control of chemical transformations.

One strong advantage of FCS is the naturally multiplexed information that can be gathered in a kinetics experiment. The identifying features of reactants, intermediates, and products can potentially be monitored within a single spectral window spanning upwards of 100 cm^{-1} depending on the methodology employed. Reaction rate coefficients can subsequently be extracted from the temporal evolution of these spectra. The measurement of coupled kinetic information – for instance the rate of decay of a reactant being equal to the rate of appearance of an intermediate – may elucidate a complex reaction potential energy surface. In addition, if all product pathways from a reaction are spectroscopically identified and their rate coefficients for production are measured, the product branching ratios can be determined. A second advantage of FCS methods is the ability to measure several spectral features of a single species at once. More precise reaction rate coefficients can be derived by monitoring multiple transitions or even an entire spectrum associated with the same molecule as a function of time.

The sheer volume of data and information contained in a single FCS kinetics experiment can appear daunting, but ultimately presents spectacular possibilities to elucidate complex chemical reaction mechanisms. Unless all molecules involved in the reaction have well-characterized spectra, then what is nominally a kinetics experiment will always require potentially high-level spectral analysis alongside kinetic data analysis. In addition, peaks may be observed that are not assigned to molecules taking part in the reaction. This abundance of spectral and kinetic data presents an exciting opportunity to fully understand chemical reactions. For example, the reaction of OD + CO → D + CO_2 is fundamental to both atmospheric and combustion chemistry, and was one of the first chemical reaction kinetics studies reported using FCS (*56*). Bjork *et al.* used CE-FCS to explicitly capture the role of the DOCO reaction intermediate for the first time. The authors measured vibrational spectra of the *cis*- and *trans*-DOCO isomers and determined their independent reaction rate coefficients for growth and decay (*103–105*). After simulating and accounting for the IR signatures of the reactants, intermediates, and products of the OD + CO → D + CO_2 reaction, additional spectral features were observed in the broadband comb spectra that did not directly involve these molecules. These peaks were ultimately accounted for by water and its isotopes, all of which have known IR spectra. The presence of a trace amount of water in both the reaction cell and the spectrum did not significantly impact the kinetic analysis.

Chemical kinetics can, of course, also be studied using more conventional direct absorption methods, including step-scan Fourier transform IR (FTIR) spectrometers, scanning narrowband lasers, or incoherent broadband light sources in combination with dispersive spectrometers. These methods have drawbacks, including limitations in achievable spectral resolution or lengthy laboratory data collection times, which can expose the study to long-timescale fluctuations. Step-scan FTIR can also achieve spectral multiplexing, but can take an order of magnitude more laboratory time to achieve the same time and spectral resolution as FCS methods (*106*, *107*). Additionally, unlike a comb, the incoherent FTIR light source cannot be efficiently coupled into an optical enhancement cavity, potentially limiting the sensitivity of the measurement.

Given the multiplexing and sensitivity advantages of FCS, along with spectral readout on the microsecond timescale, combs are being integrated into a wide variety of chemical kinetics studies. We now discuss recent case studies in the application of combs to reaction kinetics, targeting examples in both gas-phase and solution-phase environments.

2.2.1. Gas-Phase Criegee Intermediate Reaction Kinetics

Several research groups are actively applying FCS to gas-phase chemical reaction kinetics, harnessing both dual-comb and spatially dispersive methods to study reacting systems in room temperature flow cells (*56*, *58*, *108*–*113*), and high temperature flames, discharges, and shock tubes (*114*–*122*). The application of these methods to problems in atmospheric chemistry is particularly compelling. One recent room temperature FCS flow cell study by Luo *et al.* concerns the formation and subsequent reaction of the simplest Criegee intermediate, CH_2OO (*110*, *111*). Criegee intermediates are a class of zwitterions formed from the ozonolysis of alkenes, and their subsequent reactions have impacts on processes ranging from aerosol formation to the oxidative chemistry of the troposphere (*123*). Criegee chemistry has been an active area of research in atmospheric physical chemistry since 2012 when the laboratory synthetic route to forming CH_2OO was established (*124*). Since then, IR and ultraviolet (UV) absorption spectroscopies and time-of-flight mass spectrometry have been used to study the reactions of Criegee intermediates with other atmospherically relevant molecules (*125*).

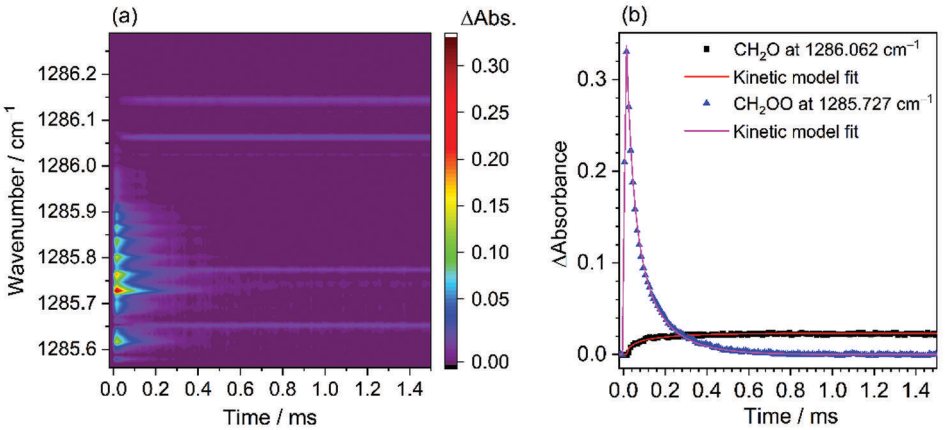


Figure 5. (a) Time-resolved DCS of Criegee chemistry near 1286 cm^{-1}. The spectra were recorded after the 248 nm irradiation of a flowing mixture of CH_2I_2/O_2 over 8000 excimer laser shots. The spectral sampling spacing was 279 MHz (9.3×10^{-3} cm^{-1}), and the temporal resolution was 10 μs. (b) Temporal profiles of a CH_2O line at 1286.062 cm^{-1} and a CH_2OO absorption peak at 1285.727 cm^{-1}. $[CH_2OO]_0$ was estimated to be 5.6×10^{13} molecule cm^{-3} by kinetic model fitting of the time traces. Adapted with permission from reference (111). Copyright 2020 The Optical Society.

The laboratory synthetic route for the formation of CH_2OO proceeds via the UV photolysis of diiodomethane (CH_2I_2) in the presence of O_2. The resulting CH_2I radical readily reacts with an excess of O_2 to form CH_2OO. The subsequent reaction of CH_2OO with other atmospherically relevant molecules is typically carried out under pseudo first-order conditions. The decay of $[CH_2OO]$ is measured as a function of time relative to the initiating photolysis laser pulse, taken to occur at $t = 0$. Luo *et al.* monitored the self-reaction of CH_2OO to form formaldehyde (CH_2O) via vibrational signatures using EO DCS in the long-wave mid-IR near 1285 cm^{-1}, shown as a function of time in Figure 5a (*110*, *111*). At short time delays following photolysis, the observed spectral peaks corresponded to the ν_4 fundamental vibrational band of CH_2OO. At longer times, part of the CH_2O

ν_6 fundamental vibrational band grew in. Whilst a fit to the whole spectrum could be used to measure the decay of [CH_2OO] and growth of [CH_2O] shown in Figure 5b, a single peak was chosen for each species. The coupled decay and growth traces of [CH_2OO] and [CH_2O] were consistent with previous kinetic models of the CH_2OO self-reaction (*126*).

It is informative to compare the capabilities of the EO DCS system of Luo *et al.* against a chirped-pulse QCL system previously used to measure the ν_4 absorption spectrum of CH_2OO (*127*). Using the QCL method, a similar spectral window of 1.5 cm^{-1} was gathered with a time resolution of 240 μs. The QCL experiments demonstrated a baseline absorbance noise level of 2.5×10^{-4} over 90 laser shots. In the DCS experiments described above, the baseline absorbance noise level was 7.1×10^{-4} when averaging a 6 μs integration time for 16,000 laser shots. Although the noise floor is somewhat higher for the DCS experiment, the time resolution is considerably better for measuring fast kinetics. In addition, the time resolution and spectral bandwidth in a DCS experiment are inherently coupled by the Nyquist criterion for a given data point spacing (*120*). The DCS experiment is therefore limited to a narrow wavelength range simply for the purposes of achieving the best time resolution (6 μs). The spectral range can be broadened with a corresponding compromise in time resolution. The central wavelength of the measurement can also be tuned over the wider 1215–1287 cm^{-1} range available to the laser system. The DCS apparatus is therefore time and frequency agile, depending on the needs of a given experiment. A more traditional step-scan FTIR instrument can also be used for CH_2OO spectroscopy and kinetics, as demonstrated by Su *et al.* (*128*) and later by Huang *et al.* (*129*) In these studies, a broader spectral bandwidth (e.g. 750–1500 cm^{-1}) was achieved using an incoherent light source while maintaining nanosecond to microsecond time resolution. However, the instrument resolution was limited to 0.25–1 cm^{-1}. Not enough information is given on noise levels to compare these experiments to EO DCS.

Long-wave mid-IR FCS experiments like the study detailed above currently rely on DCS rather than spatially dispersive methods. High-resolution dispersive optical elements and cameras operating in the long-wave mid-IR require custom fabrication and can be prohibitively expensive, although long-wave mid-IR FCS using dispersive detection was recently showcased using an immersion grating (*53*). In the short-wave mid-IR near 3000 cm^{-1}, however, dispersive comb techniques can be harnessed to study Criegee chemistry via C−H stretching signatures of the reactants, intermediates, and products.

The Lehman Research Group at the University of Leeds recently used the photolysis of CH_2I_2 and resulting laser-induced signals to commission a new dispersive frequency comb spectrometer. CH_2I_2 is a useful target when constructing a new instrument because of its large photolysis cross section ($>1\times10^{-18}$ cm^2 $molecule^{-1}$) in an easily accessible region of the UV (248–355 nm). CH_2I and CH_2 are subsequently formed in single photon and multiphoton processes, respectively. This study used a 250 MHz repetition rate mid-IR comb spanning 2700–3300 cm^{-1} and a spatially dispersive FCS spectrometer with ~35 cm^{-1} simultaneous coverage (*58*). An IR spectrum was acquired at a 400 μs time delay following photolysis (Figure 6). A spectral signature can be seen in the difference spectrum (red) of the photolysis laser on (blue) and laser off (grey) datasets. The observed peaks in the difference spectrum were almost entirely accounted for by $\sim7\times10^{13}$ molecule cm^{-3} ethylene (C_2H_4), which was modeled using its known IR absorption spectrum from the HITRAN

database (black) (*130*) convolved with the expected Doppler broadening and instrument lineshape function.

The observation of C_2H_4 was unexpected, although its presence yields insight into the experimental conditions and highlights the benefit of collecting broadband, high-resolution kinetics spectra potentially containing unknown spectral signatures. Under room temperature flow cell conditions, it is relatively easy to produce unintended reaction products if the gas refresh rate is slow compared to the photolysis laser repetition rate, as was the case here. Ethylene was likely formed from sequential photolysis laser pulses interacting with the gas sample, creating both CH_2 and CH_2I which then react to form C_2H_4. By using a broadband, high-resolution detection method with sufficient sensitivity, in addition to finding new reaction products or intermediates, any unintended reaction products or contaminant species can be identified and the experimental conditions altered.

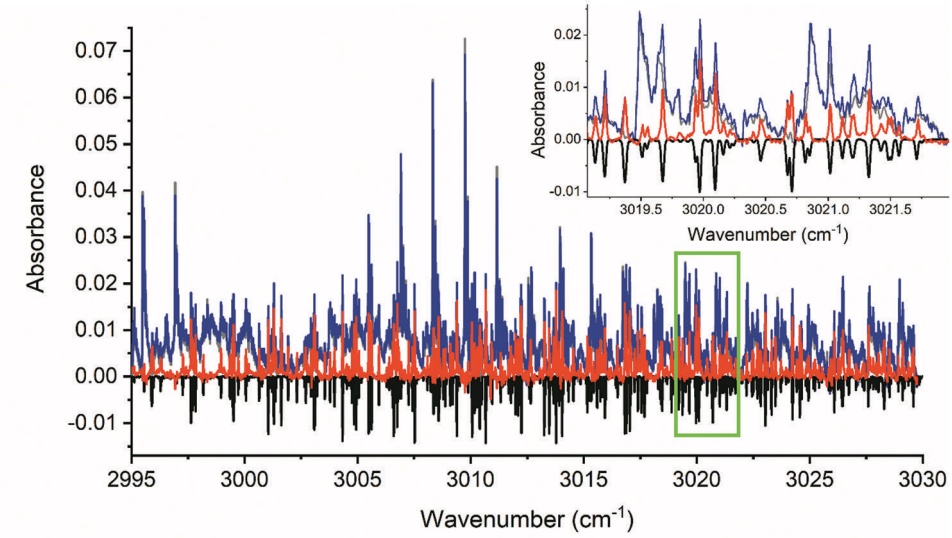


Figure 6. IR absorption spectra following the photolysis of CH_2I_2 (5×10^{16} molecule cm^{-3}, 20 mbar total pressure) at 266 nm. Spectra are shown for photolysis laser on (blue) and laser off (grey). The laser off absorption trace is dominated by CH_2I_2 features. The difference spectrum (red, photolysis laser on – laser off) is well-modeled by the C_2H_4 IR spectrum (HITRAN, black, inverted). Data were taken at 10 Hz (photolysis laser repetition rate) with 50 μs integration time at Δt(camera – photolysis laser) = 400 μs, averaging for 2000 images.

2.2.2. Liquid-Phase Monolayer Desorption Kinetics

Although the full advantages of simultaneously broadband and high-resolution frequency comb light sources are perhaps most ideally matched to gas-phase studies, where linewidths are typically limited by Doppler broadening, there have been a number of successful liquid-phase studies employing DCS methods (*106*, *107*, *131–138*). Since the achievable spectral resolution in condensed phase spectroscopy is usually governed by inhomogeneous solvent interactions rather than instrument limitations, larger comb repetition rates are sufficient. Major applications of DCS to liquid-phase kinetics range from simple organic reactions (*133*) to irreversible protein reactions (*107*, *134*).

DCS has been employed in attenuated total reflectance (ATR) spectrometers, used for studying liquid-phase reactions and monolayer deposition processes (*106*, *133*). Lins *et al*. recently studied the spectroelectrochemistry of the desorption of a monolayer of a pyridine derivative (*106*). A commercial QCL-based DCS instrument was coupled into an ATR-surface-enhanced IR absorption spectroscopy (SEIRAS) accessory, which was adapted for a laser light source instead of the usual broadband incoherent light source. The authors prepared a gold nanoparticle film on top of an indium tin oxide layered silicon internal reflection element, and adsorbed a monolayer of 4-dimethylaminopyridine (DMAP). Whilst this pyridine derivative was chosen as a proof-of-concept target, its use in organic films and molecular devices is well documented (*139*, *140*). DMAP was desorbed from the gold surface by applying a potential jump, and the 1610–1670 cm^{-1} IR spectrum was collected as a function of time (Figure 7). The transient IR signal observed near 1628 cm^{-1} was assigned to several ring vibrational modes of DMAP. The decrease in absorbance signal showed evidence for the desorption process, allowing for the measurement of time constants for the desorption of DMAP from gold and its subsequent diffusion.

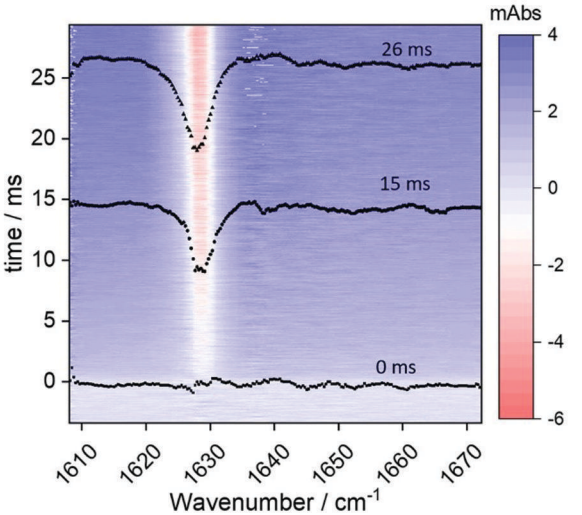


Figure 7. Time-resolved evolution of the ATR-SEIRAS absorbance change upon DMAP desorption from a gold surface, following a potential jump from +0.30 to −0.90 V, acquired using a mid-IR dual-comb spectrometer. Spectral processing conditions were 128 coadditions with 20 μs time binning. Spectral resolution was 3.3 cm^{-1}. Reproduced with permission from reference (*106*). *Copyright 2020 American Chemical Society.*

The study by Lins *et al*. demonstrates the potential for ATR DCS to replace step-scan FTIR ATR-SEIRAS. The detection limit of the DCS experiment was approximately 0.08 mAbs, or 0.7% of the monolayer, using a time resolution of 800 μs and spectral resolution of 3.3 cm^{-1}. A step-scan FTIR spectrometer can achieve similar sensitivity and time resolution with a lower 8 cm^{-1} spectral resolution. The most striking point of comparison, however, is the laboratory time necessary to achieve these levels of sensitivity with comparable temporal resolution. Conventional step-scan FTIR requires the equivalent of 2 days of laboratory time, while the DCS experiment takes 32 minutes. The implementation of DCS by Lins *et al.* used a QCL operating over a much smaller spectral window compared to the broadband incoherent light source used in conventional methods.

However, DCS clearly has an enormous advantage in laboratory time if the target wavelength for a given experiment falls within the QCL operating wavelength range.

2.3. Molecular Sensing

We finally turn our attention to implementations of FCS for analytical sensing. Here we define sensing as the identification and quantification of steady-state concentrations of molecules present in a mixture using known spectral signatures. Molecular sensing is a robust application of FCS with huge potential across many different fields (*116*, *141–153*) due to the unique attributes of comb instrumentation already emphasized throughout this Chapter. The analytical chemistry applications of FCS include characterizing emissions in storage facilities (*144*), accurately measuring temperatures and quality factors of combustion environments (*116*, *152*), and human breath analysis for medical diagnostics (*35*, *154*, *155*). The success and widespread adoption of combs for sensing are highly dependent on rapidly developing technological advances, as discussed by Ycas *et al.* (*143*) and references therein. Sensing applications also show significant promise in introducing combs to a broader scientific audience and the general public.

A distinct advantage of FCS – and laser absorption spectroscopy techniques more generally – for sensing is the highly directional nature of their detection and the potential for long distance propagation (*156*). This enables long-path measurements, including atmospheric monitoring of pollutants and tracking natural gas leaks across a large open field (*148*, *149*, *153*). FCS is also calibration-free and allows for simultaneous monitoring of numerous molecules. As we have discussed throughout this Chapter, FCS can be used to probe various environments under a wide range of experimental conditions.

FCS, particularly DCS methodology, has made significant strides in becoming compact, user-friendly, and field-deployable with low power consumption (*143*). These are attractive qualities to position DCS as a viable alternative to other passive sensing techniques. In addition, technological advances in comb and fiber technology enable researchers to access the chemically important mid-IR in field-deployable instrumentation while still covering a broadband spectral range. These instruments are therefore no longer limited to probing weak vibrational overtones in the near-IR nor are they limited to laboratory environments. To give a specific example, Ycas *et al.* measured concentrations of volatile organic compounds (VOCs) including ethane and propane in open-path field experiments using a DCS instrument spanning 2750–3150 cm^{-1} with 0.0067 cm^{-1} resolution. After signal processing, this new instrument achieved a sensitivity dependent on the path length and integration time of $120\ ppb \cdot m \cdot \sqrt{minutes}$ (*143*). Continuous measurements of up to 30 hours of data were taken for a 120 m open path, highlighting the stability of this instrumentation.

Depending on the molecular targets, it might seem challenging to outpace cost-effective and user-friendly techniques such as chemometric and eNose sensors, or the highly sensitive established techniques of chromatography and mass spectrometry (*157*). The UK Department for Environment Food & Rural Affairs (Defra) serves as a useful benchmark. Defra uses Perkin Elmer Ozone Precursor gas chromatography-flame ionization detector systems stationed at multiple locations as part of their automated hydrocarbon monitoring network. Hourly measurements of concentrations of close to 30 different VOCs are taken by sampling the air at the instrumentation site (*158*). This chromatography instrument has limits of detection in the low parts-per-billion (<0.1 ppb) for various VOC pollutants, but needs to be calibrated using a gas mixture standard. The mid-IR field-deployable DCS instrument of Ycas *et al*. can reach the ppb sensitivity necessary to monitor atmospheric VOCs, similar to the more conventional chromatography methods but without the need for calibration.

Moreover, the DCS instrumentation can take continuous, open-path measurements in a directional manner, yielding VOC concentration and identification profiles as a function of location and time. This capability may prove of extreme utility in industrial settings as well as for environmental monitoring and atmospheric modeling of tropospheric chemistry (*159*, *160*).

3. Conclusions and Outlook

In this Chapter, we have surveyed the current state of frequency comb spectroscopy and its myriad applications in observing and understanding chemical phenomena. It is now demonstrated that combs can replace incoherent and narrowband light sources in most direct absorption spectroscopy experiments, improving the precision and sensitivity of these measurements as well as the laboratory timescales for data collection.

Frequency combs have enabled great strides forward in fundamental laboratory spectroscopy and dynamics. We reviewed several recent high-impact studies where the capabilities of FCS infrastructure have elucidated the structure of challenging spectroscopic targets that proved inaccessible with other techniques. Combs are of particular utility for precision spectroscopy, with frequency resolution unconstrained by instrument lineshapes. In combination with cryogenic buffer gas cooling techniques, FCS has enabled state-resolved measurements of unprecedentedly large fullerene molecules. The size limit for quantum state resolution has certainly not yet been reached; moving to lower internal temperatures with improved cooling and longer mid-IR wavelengths should permit the study of even larger systems. The applications of direct comb methods for ion spectroscopy and sub-Doppler measurements are similarly not far past the proof-of-concept stage, and can be extended to considerably more complex molecular species of broad chemical interest. The realization of frequency combs as femtosecond light sources that can be resonantly coupled to optical cavities has ushered in a new era of all-optical ultrasensitive, ultrafast measurements in dilute gas-phase samples.

Combs are also now widely applied to probe chemical reaction kinetics on the microsecond to millisecond timescale in both gas- and liquid-phase environments. We highlighted particular applications in atmospheric chemistry and monolayer desorption experiments to showcase their utility across various fields of chemistry. Kinetics measurements under extreme conditions can inform our understanding of chemistry in environments ranging from combustion engines to regions of the interstellar medium. Low temperature kinetics studies can provide detailed information on reaction potential energy surfaces, such as the presence of submerged or low-lying barriers to reaction. Low temperature experiments are currently under construction in at least two different research groups at the University of Leeds and the Université de Rennes, combining a cold molecular flow produced using a Laval expansion with FCS detection (*161*). The future of comb-based chemical reaction kinetics could see expansion of chemical applications or the use of alternative spectroscopic probes including THz radiation (*113*).

Outside of the physical chemistry laboratory, molecular sensing will likely become a highly successful application of FCS, particularly with the development of lower cost, miniaturized systems. In this Chapter, we emphasized the recent use of FCS for open-path environmental monitoring measurements. Novel sensing applications may include the integration of FCS as a passive in-line spectroscopic probe of industrial scale flow chemistry (*162*) or as a hospital bedside breath gas analyzer aimed at identifying biosignatures for disease diagnosis (*163*). Further development of FCS technologies surrounding sensing applications are likely to result in broader scientific and general public involvement, creating a feedback loop of investment and technological expansion.

Optical frequency combs have proved to be powerful spectroscopic tools due to their precision, bandwidth, potential for high sensitivity measurements, and rapid experimental readout times. The ability to collect multiplexed information in a single experiment is a significant advantage in many of the applications discussed herein. At present, save for a few high-impact spectroscopic and kinetics studies, most of the recent chemical applications of FCS are proof-of-concept or benchmarking experiments. As comb technology matures and reaches more laboratories, we expect that an accompanying expansion of chemical applications will become evident. We anticipate that the coming years will yield new comb-based demonstrations of precision spectroscopy for tests of fundamental physics, resolved sub-Doppler structure in unprecedentedly complex molecular systems, sensitive probes of cold chemistry and kinetics, new limits on the detection of ultrafast reaction dynamics, and integration with microscopy for applications in biology and nanoscience.

References

1. Hall, J. L. Nobel Lecture: Defining and Measuring Optical Frequencies. *Rev. Mod. Phys.* **2006**, *78*, 1279–1295.
2. Hänsch, T. W. Nobel Lecture: Passion for Precision. *Rev. Mod. Phys.* **2006**, *78*, 1297–1309.
3. Cundiff, S. T.; Ye, J. Femtosecond Optical Frequency Combs. *Rev. Mod. Phys.* **2003**, *75*, 325–342.
4. Diddams, S. A. The Evolving Optical Frequency Comb. *J. Opt. Soc. Am. B* **2010**, *27*, B51–B62.
5. Fortier, T.; Baumann, E. 20 Years of Developments in Optical Frequency Comb Technology and Applications. *Commun. Phys.* **2019**, *2*, 16.
6. Diddams, S. A.; Vahala, K.; Udem, T. Optical Frequency Combs: Coherently Uniting the Electromagnetic Spectrum. *Science* **2020**, *369*, eaay3676.
7. Adler, F.; Thorpe, M. J.; Cossel, K. C.; Ye, J. Cavity-Enhanced Direct Frequency Comb Spectroscopy: Technology and Applications. *Annu. Rev. Anal. Chem.* **2010**, *3*, 175–205.
8. Weichman, M. L.; Changala, P. B.; Ye, J.; Chen, Z.; Yan, M.; Picqué, N. Broadband Molecular Spectroscopy with Optical Frequency Combs. *J. Mol. Spectrosc.* **2019**, *355*, 66–78.
9. Picqué, N.; Hänsch, T. W. Frequency Comb Spectroscopy. *Nat. Photonics* **2019**, *13*, 146–157.
10. Cossel, K. C.; Waxman, E. M.; Finneran, I. A.; Blake, G. A.; Ye, J.; Newbury, N. R. Gas-Phase Broadband Spectroscopy Using Active Sources: Progress, Status, and Applications. *J. Opt. Soc. Am. B* **2017**, *34*, 104–129.
11. Jones, D. J.; Diddams, S. A.; Ranka, J. K.; Stentz, A.; Windeler, R. S.; Hall, J. L.; Cundiff, S. T. Carrier-Envelope Phase Control of Femtosecond Mode-Locked Lasers and Direct Optical Frequency Synthesis. *Science* **2000**, *288*, 635–639.
12. Reichert, J.; Niering, M.; Holzwarth, R.; Weitz, M.; Udem, T.; Hänsch, T. W. Phase Coherent Vacuum-Ultraviolet to Radio Frequency Comparison with a Mode-Locked Laser. *Phys. Rev. Lett.* **2000**, *84*, 3232–3235.
13. Schliesser, A.; Picqué, N.; Hänsch, T. W. Mid-Infrared Frequency Combs. *Nat. Photonics* **2012**, *6*, 440–449.
14. Kim, J.; Song, Y. J. Ultralow-Noise Mode-Locked Fiber Lasers and Frequency Combs: Principles, Status, and Applications. *Adv. Opt. Photonics* **2016**, *8*, 465–540.
15. Sinclair, L. C.; Deschenes, J.-D.; Sonderhouse, L.; Swann, W. C.; Khader, I. H.; Baumann, E.; Newbury, N. R.; Coddington, I. Invited Article: A Compact Optically Coherent Fiber Frequency Comb. *Rev. Sci. Instrum.* **2015**, *86*, 081301.

16. Adler, F.; Cossel, K. C.; Thorpe, M. J.; Hartl, I.; Fermann, M. E.; Ye, J. Phase-Stabilized, 1.5 W Frequency Comb at 2.8-4.8 μm. *Opt. Lett.* **2009**, *34*, 1330–1332.
17. Meek, S.; Poisson, A.; Guelachvili, G.; Hänsch, T. W.; Picqué, N. Fourier Transform Spectroscopy Around 3 μm with a Broad Difference Frequency Comb. *Appl. Phys. B* **2014**, *114*, 573–578.
18. Lee, K. F.; Hensley, C. J.; Schunemann, P. G.; Fermann, M. E. Midinfrared Frequency Comb by Difference Frequency of Erbium and Thulium Fiber Lasers in Orientation-Patterned Gallium Phosphide. *Opt. Express* **2017**, *25*, 17411–17416.
19. Iwakuni, K.; Porat, G.; Bui, T. Q.; Bjork, B. J.; Schoun, S. B.; Heckl, O. H.; Fermann, M. E.; Ye, J. Phase-Stabilized 100 mW Frequency Comb Near 10 mm. *Appl. Phys. B* **2018**, *124*, 128.
20. Muraviev, A. V.; Smolski, V. O.; Loparo, Z. E.; Vodopyanov, K. L. Massively Parallel Sensing of Trace Molecules and Their Isotopologues with Broadband Subharmonic Mid-Infrared Frequency Combs. *Nat. Photonics* **2018**, *12*, 209–214.
21. Timmers, H.; Kowligy, A.; Lind, A.; Cruz, F. C.; Nader, N.; Silfies, M.; Ycas, G.; Allison, T. K.; Schunemann, P. G.; Papp, S. B.; Diddams, S. A. Molecular Fingerprinting with Bright, Broadband Infrared Frequency Combs. *Optica* **2018**, *5*, 727–732.
22. Chen, Y.; Silfies, M. C.; Kowzan, G.; Bautista, J. M.; Allison, T. K. Tunable Visible Frequency Combs from a Yb-Fiber-Laser-Pumped Optical Parametric Oscillator. *Appl. Phys. B* **2019**, *125*, 81.
23. Lesko, D. M. B.; Timmers, H.; Xing, S.; Kowligy, A.; Lind, A. J.; Diddams, S. A. A Six-Octave Optical Frequency Comb from a Scalable Few-Cycle Erbium Fibre Laser. *Nat. Photonics* **2021**, *15*, 281.
24. Pupeza, I.; Zhang, C.; Högner, M.; Ye, J. Extreme-Ultraviolet Frequency Combs for Precision Metrology and Attosecond Science. *Nat. Photonics* **2021**, *15*, 175–186.
25. Kippenberg, T. J.; Holzwarth, R.; Diddams, S. A. Microresonator-Based Optical Frequency Combs. *Science* **2011**, *332*, 555–559.
26. Herr, T.; Brasch, V.; Jost, J. D.; Wang, C. Y.; Kondratiev, N. M.; Gorodetsky, M. L.; Kippenberg, T. J. Temporal Solitons in Optical Microresonators. *Nat. Photonics* **2014**, *8*, 145–152.
27. Brasch, V.; Lucas, E.; Jost, J. D.; Geiselmann, M.; Kippenberg, T. J. Self-Referenced Photonic Chip Soliton Kerr Frequency Comb. *Light-Sci. Appl.* **2017**, *6*, e16202.
28. Suh, M.-G.; Yang, Q.-F.; Yang, K. Y.; Yi, X.; Vahala, K. J. Microresonator Soliton Dual-Comb Spectroscopy. *Science* **2016**, *354*, 600–603.
29. Parriaux, A.; Hammani, K.; Millot, G. Electro-Optic Frequency Combs. *Adv. Opt. Photonics* **2020**, *12*, 223–287.
30. Carlson, D. R.; Hickstein, D. D.; Zhang, W.; Metcalf, A. J.; Quinlan, F.; Diddams, S. A.; Papp, S. B. Ultrafast Electro-Optic Light with Subcycle Control. *Science* **2018**, *361*, 1358–1362.
31. Kazakov, D.; Piccardo, M.; Wang, Y.; Chevalier, P.; Mansuripur, T. S.; Xie, F.; Zah, C.-e.; Lascola, K.; Belyanin, A.; Capasso, F. Self-Starting Harmonic Frequency Comb Generation in a Quantum Cascade Laser. *Nat. Photonics* **2017**, *11*, 789–792.
32. Hillbrand, J.; Andrews, A. M.; Detz, H.; Strasser, G.; Schwarz, B. Coherent Injection Locking of Quantum Cascade Laser Frequency Combs. *Nat. Photonics* **2019**, *13*, 101–104.

33. Villares, G.; Hugi, A.; Blaser, S.; Faist, J. Dual-Comb Spectroscopy Based on Quantum-Cascade-Laser Frequency Combs. *Nat. Commun* **2014**, *5*, 5192.
34. Sterczewski, L. A.; Westberg, J.; Bagheri, M.; Frez, C.; Vurgaftman, I.; Canedy, C. L.; Bewley, W. W.; Merritt, C. D.; Kim, C. S.; Kim, M.; Meyer, J. R.; Wysocki, G. Mid-Infrared Dual-Comb Spectroscopy with Interband Cascade Lasers. *Opt. Lett.* **2019**, *44*, 2113–2116.
35. Thorpe, M. J.; Balslev-Clausen, D.; Kirchner, M. S.; Ye, J. Cavity-Enhanced Optical Frequency Comb Spectroscopy: Application to Human Breath Analysis. *Opt. Express* **2008**, *16*, 2387–2397.
36. Masłowski, P.; Cossel, K. C.; Foltynowicz, A.; Ye, J. Cavity-Enhanced Direct Frequency Comb Spectroscopy. In *Cavity-Enhanced Spectroscopy and Sensing*; Gagliardi, G., Loock, H.-P. , Eds.; Springer: Berlin, Heidelberg, 2014; pp 271-321.
37. Mandon, J.; Guelachvili, G.; Picqué, N. Fourier Transform Spectroscopy with a Laser Frequency Comb. *Nat. Photonics* **2009**, *3*, 99–102.
38. Foltynowicz, A.; Ban, T.; Masłowski, P.; Adler, F.; Ye, J. Quantum-Noise-Limited Optical Frequency Comb Spectroscopy. *Phys. Rev. Lett.* **2011**, *107*, 233002.
39. Masłowski, P.; Lee, K. F.; Johansson, A. C.; Khodabakhsh, A.; Kowzan, G.; Rutkowski, L.; Mills, A. A.; Mohr, C.; Jiang, J.; Fermann, M. E.; Foltynowicz, A. Surpassing the Path-Limited Resolution of Fourier-Transform Spectrometry with Frequency Combs. *Phys. Rev. A* **2016**, *93*, 021802.
40. Coddington, I.; Newbury, N.; Swann, W. Dual-Comb Spectroscopy. *Optica* **2016**, *3*, 414–426.
41. Long, D. A.; Fleisher, A. J.; Douglass, K. O.; Maxwell, S. E.; Bielska, K.; Hodges, J. T.; Plusquellic, D. F. Multiheterodyne Spectroscopy with Optical Frequency Combs Generated from a Continuous-Wave Laser. *Opt. Lett.* **2014**, *39*, 2688–2690.
42. Fleisher, A. J.; Long, D. A.; Reed, Z. D.; Hodges, J. T.; Plusquellic, D. F. Coherent Cavity-Enhanced Dual-Comb Spectroscopy. *Opt. Express* **2016**, *24*, 10424–10434.
43. Znakovskaya, I.; Fill, E.; Forget, N.; Tournois, P.; Seidel, M.; Pronin, O.; Krausz, F.; Apolonski, A. Dual Frequency Comb Spectroscopy with a Single Laser. *Opt. Lett.* **2014**, *39*, 5471–5474.
44. Carlson, D. R.; Hickstein, D. D.; Cole, D. C.; Diddams, S. A.; Papp, S. B. Dual-Comb Interferometry via Repetition Rate Switching of a Single Frequency Comb. *Opt. Lett.* **2018**, *43*, 3614–3617.
45. Fellinger, J.; Mayer, A. S.; Winkler, G.; Grosinger, W.; Truong, G.-W.; Droste, S.; Li, C.; Heyl, C. M.; Hartl, I.; Heckl, O. H. Tunable Dual-Comb from an All-Polarization-Maintaining Single-Cavity Dual-Color Yb:fiber Laser. *Opt. Express* **2019**, *27*, 28062–28074.
46. Liao, R.; Tian, H.; Liu, W.; Li, R.; Song, Y.; Hu, M. Dual-Comb Generation from a Single Laser Source: Principles and Spectroscopic Applications Towards Mid-IR: A Review. *J. Phys.-Photonics* **2020**, *2*, 042006.
47. Roy, J.; Deschênes, J. D.; Potvin, S.; Genest, J. Continuous Real-Time Correction and Averaging for Frequency Comb Interferometry. *Opt. Express* **2012**, *20*, 21932–21939.
48. Deschênes, J. D.; Genest, J. Frequency-Noise Removal and On-Line Calibration for Accurate Frequency Comb Interference Spectroscopy of Acetylene. *Appl. Optics* **2014**, *53*, 731–735.

49. Ideguchi, T.; Poisson, A.; Guelachvili, G.; Picqué, N.; Hänsch, T. W. Adaptive Real-Time Dual-Comb Spectroscopy. *Nat. Commun.* **2014**, *5*, 3375.
50. Sterczewski, L. A.; Westberg, J.; Wysocki, G. Computational Coherent Averaging for Free-Running Dual-Comb Spectroscopy. *Opt. Express* **2019**, *27*, 23875–23893.
51. Sterczewski, Ł. A.; Przewłoka, A.; Kaszub, W.; Sotor, J. Computational Doppler-Limited Dual-Comb Spectroscopy with a Free-Running All-Fiber Laser. *Appl. Photonics* **2019**, *4*, 116102.
52. Nugent-Glandorf, L.; Neely, T.; Adler, F.; Fleisher, A. J.; Cossel, K. C.; Bjork, B.; Dinneen, T.; Ye, J.; Diddams, S. A. Mid-Infrared Virtually Imaged Phased Array Spectrometer for Rapid and Broadband Trace Gas Detection. *Opt. Lett.* **2012**, *37*, 3285–3287.
53. Iwakuni, K.; Bui, T. Q.; Niedermeyer, J. F.; Sukegawa, T.; Ye, J. Comb-Resolved Spectroscopy with Immersion Grating in Long-Wave Infrared. *Opt. Express* **2019**, *27*, 1911–1921.
54. Diddams, S. A.; Hollberg, L.; Mbele, V. Molecular Fingerprinting with the Resolved Modes of a Femtosecond Laser Frequency Comb. *Nature* **2007**, *445*, 627–630.
55. Karim, F.; Scholten, S. K.; Perrella, C.; Luiten, A. N. Ultrahigh-Resolution Direct-Frequency-Comb Spectrometer. *Phys. Rev. Appl.* **2020**, *14*, 8.
56. Bjork, B. J.; Bui, T. Q.; Heckl, O. H.; Changala, P. B.; Spaun, B.; Heu, P.; Follman, D.; Deutsch, C.; Cole, G. D.; Aspelmeyer, M.; Okumura, M.; Ye, J. Direct Frequency Comb Measurement of OD + CO → DOCO Kinetics. *Science* **2016**, *354*, 444–448.
57. Bailey, D. M.; Zhao, G.; Fleisher, A. J. Precision Spectroscopy of Nitrous Oxide Isotopocules with a Cross-Dispersed Spectrometer and a Mid-Infrared Frequency Comb. *Anal. Chem.* **2020**, *92*, 13759–13766.
58. Roberts, F. C.; Lewandowski, H. J.; Hobson, B. F.; Lehman, J. H. A Rapid, Spatially Dispersive Frequency Comb Spectrograph Aimed at Gas Phase Chemical Reaction Kinetics. *Mol. Phys.* **2020**, *118*, e1733116.
59. Finneran, I. A.; Good, J. T.; Holland, D. B.; Carroll, P. B.; Allodi, M. A.; Blake, G. A. Decade-Spanning High-Precision Terahertz Frequency Comb. *Phys. Rev. Lett.* **2015**, *114*, 163902.
60. Kowligy, A. S.; Timmers, H.; Lind, A. J.; Elu, U.; Cruz, F. C.; Schunemann, P. G.; Biegert, J.; Diddams, S. A. Infrared Electric Field Sampled Frequency Comb Spectroscopy. *Sci. Adv.* **2019**, *5*, eaaw8794.
61. Gohle, C.; Stein, B.; Schliesser, A.; Udem, T.; Hänsch, T. W. Frequency Comb Vernier Spectroscopy for Broadband, High-Resolution, High-Sensitivity Absorption and Dispersion Spectra. *Phys. Rev. Lett.* **2007**, *99*, 263902.
62. Khodabakhsh, A.; Ramaiah-Badarla, V.; Rutkowski, L.; Johansson, A. C.; Lee, K. F.; Jiang, J.; Mohr, C.; Fermann, M. E.; Foltynowicz, A. Fourier Transform and Vernier Spectroscopy using an Optical Frequency Comb at 3-5.4 mm. *Opt. Lett.* **2016**, *41*, 2541–2544.
63. Sadiek, I.; Mikkonen, T.; Vainio, M.; Toivonen, J.; Foltynowicz, A. Optical Frequency Comb Photoacoustic Spectroscopy. *Phys. Chem. Chem. Phys.* **2018**, *20*, 27849–27855.
64. Friedlein, J. T.; Baumann, E.; Briggman, K. A.; Colacion, G. M.; Giorgetta, F. R.; Goldfain, A. M.; Herman, D. I.; Hoenig, E. V.; Hwang, J.; Newbury, N. R.; Perez, E. F.; Yung, C. S.; Coddington, I.; Cossel, K. C. Dual-Comb Photoacoustic Spectroscopy. *Nat. Commun.* **2020**, *11*, 10.

65. Wildi, T.; Voumard, T.; Brasch, V.; Yilmaz, G.; Herr, T. Photo-Acoustic Dual-Frequency Comb Spectroscopy. *Nat. Commun.* **2020**, *11*, 4164.
66. Reber, M. A. R.; Chen, Y.; Allison, T. K. Cavity-Enhanced Ultrafast Spectroscopy: Ultrafast Meets Ultrasensitive. *Optica* **2016**, *3*, 311–317.
67. Morgenweg, J.; Barmes, I.; Eikema, K. S. E. Ramsey-Comb Spectroscopy with Intense Ultrashort Laser Pulses. *Nat. Phys.* **2014**, *10*, 30–33.
68. Ding, S.; Matsukevich, D. N. Quantum Logic for the Control and Manipulation of Molecular Ions using a Frequency Comb. *New J. Phys.* **2012**, *14*, 023028.
69. Chou, C. W.; Collopy, A. L.; Kurz, C.; Lin, Y.; Harding, M. E.; Plessow, P. N.; Fortier, T.; Diddams, S.; Leibfried, D.; Leibrandt, D. R. Frequency-Comb Spectroscopy on Pure Quantum States of a Single Molecular Ion. *Science* **2020**, *367*, 1458–1461.
70. Hébert, N. B.; Scholten, S. K.; White, R. T.; Genest, J.; Luiten, A. N.; Anstie, J. D. A Quantitative Mode-Resolved Frequency Comb Spectrometer. *Opt. Express* **2015**, *23*, 13991–14001.
71. Spaun, B.; Changala, P. B.; Patterson, D.; Bjork, B. J.; Heckl, O. H.; Doyle, J. M.; Ye, J. Continuous Probing of Cold Complex Molecules with Infrared Frequency Comb Spectroscopy. *Nature* **2016**, *533*, 517–520.
72. Changala, P. B.; Spaun, B.; Patterson, D.; Doyle, J. M.; Ye, J. Sensitivity and Resolution in Frequency Comb Spectroscopy of Buffer Gas Cooled Polyatomic Molecules. *Appl. Phys. B* **2016**, *122*, 292.
73. *Cavity-Enhanced Spectroscopy and Sensing*; Springer, 2014.
74. Changala, P. B.; Weichman, M. L.; Lee, K. F.; Fermann, M. E.; Ye, J. Rovibrational Quantum State Resolution of the C_{60} Fullerene. *Science* **2019**, *363*, 49–54.
75. Berera, R.; van Grondelle, R.; Kennis, J. T. M. Ultrafast Transient Absorption Spectroscopy: Principles and Application to Photosynthetic Systems. *Photosynth. Res.* **2009**, *101*, 105–118.
76. Schriever, C.; Lochbrunner, S.; Riedle, E.; Nesbitt, D. J. Ultrasensitive Ultraviolet-Visible 20 fs Absorption Spectroscopy of Low Vapor Pressure Molecules in the Gas Phase. *Rev. Sci. Instrum.* **2008**, *79*, 013107.
77. Silfies, M. C.; Kowzan, G.; Chen, Y. N.; Lewis, N.; Hou, R.; Baehre, R.; Gross, T.; Allison, T. K. Widely Tunable Cavity-Enhanced Frequency Combs. *Opt. Lett.* **2020**, *45*, 2123–2126.
78. Silfies, M. C.; Kowzan, G.; Lewis, N.; Allison, T. K. Broadband Cavity-Enhanced Ultrafast Spectroscopy. *Phys. Chem. Chem. Phys.* **2021**, *23*, 9743–9752.
79. Lomsadze, B.; Cundiff, S. T. Frequency Combs Enable Rapid and High-Resolution Multidimensional Coherent Spectroscopy. *Science* **2017**, *357*, 1389–1391.
80. Lomsadze, B.; Smith, B. C.; Cundiff, S. T. Tri-comb spectroscopy. *Nat. Photonics* **2018**, *12*, 676–680.
81. Allison, T. K. Cavity-Enhanced Ultrafast Two-Dimensional Spectroscopy Using Higher Order Modes. *J. Phys. B-At. Mol. Opt.* **2017**, *50*, 044004.
82. Snow, T. P.; Bierbaum, V. M. Ion Chemistry in the Interstellar Medium. *Annu. Rev. Anal. Chem.* **2008**, *1*, 229–259.
83. McGuire, B. A.; Asvany, O.; Brünken, S.; Schlemmer, S. Laboratory Spectroscopy Techniques to Enable Observations of Interstellar Ion Chemistry. *Nat. Rev. Phys.* **2020**, *2*, 402–410.

84. Puri, P.; Mills, M.; Schneider, C.; Simbotin, I.; Montgomery, J. A.; Cote, R.; Suits, A. G.; Hudson, E. R. Synthesis of Mixed Hypermetallic Oxide $BaOCa^+$ from Laser-Cooled Reagents in an Atom-Ion Hybrid Trap. *Science* **2017**, *357*, 1370–+.
85. Cairncross, W. B.; Gresh, D. N.; Grau, M.; Cossel, K. C.; Roussy, T. S.; Ni, Y.; Zhou, Y.; Ye, J.; Cornell, E. A. Precision Measurement of the Electron's Electric Dipole Moment using Trapped Molecular Ions. *Phys. Rev. Lett.* **2017**, *119*, 153001.
86. Chou, C.-W.; Kurz, C.; Hume, D. B.; Plessow, P. N.; Leibrandt, D. R.; Leibfried, D. Preparation and Coherent Manipulation of Pure Quantum States of a Single Molecular Ion. *Nature* **2017**, *545*, 203–+.
87. Asvany, O.; Krieg, J.; Schlemmer, S. Frequency Comb Assisted Mid-Infrared Spectroscopy of Cold Molecular Ions. *Rev. Sci. Instrum.* **2012**, *83*, 093110.
88. Jusko, P.; Konietzko, C.; Schlemmer, S.; Asvany, O. Frequency Comb Assisted Measurement of Fundamental Transitions of Cold H_3^+, H_2D^+ and D_2H^+. *J. Mol. Spectrosc.* **2016**, *319*, 55–58.
89. Asvany, O.; Yamada, K. M. T.; Brünken, S.; Potapov, A.; Schlemmer, S. Experimental Ground-State Combination Differences of CH_5^+. *Science* **2015**, *347*, 1346–1349.
90. Markus, C. R.; McCall, B. J. Highly Accurate Experimentally Determined Energy Levels of H_3^+. *J. Chem. Phys.* **2019**, *150*, 214303.
91. Sinclair, L. C.; Cossel, K. C.; Coffey, T.; Ye, J.; Cornell, E. A. Frequency Comb Velocity-Modulation Spectroscopy. *Phys. Rev. Lett.* **2011**, *107*, 093002.
92. Gresh, D. N.; Cossel, K. C.; Zhou, Y.; Ye, J.; Cornell, E. A. Broadband Velocity Modulation Spectroscopy of ThF^+ for Use in a Measurement of the Electron Electric Dipole Moment. *J. Mol. Spectrosc.* **2016**, *319*, 1–9.
93. Foltynowicz, A.; Rutkowski, L.; Silander, I.; Johansson, A. C.; de Oliveira, V. S.; Axner, O.; Soboń, G.; Martynkien, T.; Mergo, P.; Lehmann, K. K. Sub-Doppler Double-Resonance Spectroscopy of Methane using a Frequency Comb Probe. *Phys. Rev. Lett.* **2021**, *126*, 063001.
94. Foltynowicz, A.; Rutkowski, L.; Silander, I.; Johansson, A. C.; de Oliveira, V. S.; Axner, O.; Soboń, G.; Martynkien, T.; Mergo, P.; Lehmann, K. K. Measurement and Assignment of Double-Resonance Transitions to the 8900-9100-cm^{-1} Levels of Methane. *Phys. Rev. A* **2021**, *103*, 022810.
95. Hargreaves, R. J.; Gordon, I. E.; Rey, M.; Nikitin, A. V.; Tyuterev, V. G.; Kochanov, R. V.; Rothman, L. S. An Accurate, Extensive, and Practical Line List of Methane for the HITEMP Database. *Astrophys. J. Suppl. S* **2020**, *247*, 55.
96. Kocheril, P. A.; Markus, C. R.; Esposito, A. M.; Schrader, A. W.; Dieter, T. S.; McCall, B. J. Extended Sub-Doppler Resolution Spectroscopy of the ν_3 Band of Methane. *J. Quant. Spectrosc. Radiat. Transf.* **2018**, *215*, 9–12.
97. Hu, C. L.; Perevalov, V. I.; Cheng, C. F.; Hua, T.-P.; Liu, A.-W.; Sun, Y. R.; Tan, Y.; Wang, J.; Hu, S.-M. Optical-Optical Double-Resonance Absorption Spectroscopy of Molecules with Kilohertz Accuracy. *J. Phys. Chem. Lett.* **2020**, *11*, 7843–7848.
98. Okubo, S.; Inaba, H.; Okuda, S.; Sasada, H. Frequency Measurements of the $2\nu_3$ A_1-ν_3 Band Transitions of Methane in Comb-Referenced Infrared-Infrared Double-Resonance Spectroscopy. *Phys. Rev. A* **2021**, *103*, 022809.

99. Long, D. A.; Fleisher, A. J.; Plusquellic, D. F.; Hodges, J. T. Multiplexed Sub-Doppler Spectroscopy with an Optical Frequency Comb. *Phys. Rev. A* **2016**, *94*, 061801.
100. Chevalier, M.; De Martino, A. Double-Resonance Observation of the ($3n_3$, F_1) State of Methane. *Chem. Phys. Lett.* **1987**, *135*, 446–450.
101. Bañares, M. A.; Guerrero-Pérez, M. O.; Fierro, J. L. G.; Cortez, G. G. Raman Spectroscopy during Catalytic Operations with On-Line Activity Measurement (Operando Spectroscopy): A Method for Understanding the Active Centres of Cations Supported on Porous Materials. *J. Mater. Chem.* **2002**, *12*, 3337–3342.
102. Kohse-Höinghaus, K.; Troe, J.; Grabow, J.-U.; Olzmann, M.; Friedrichs, G.; Hungenberg, K.-D. Kinetics in the Real World: Linking Molecules, Processes, and Systems. *Phys. Chem. Chem. Phys.* **2018**, *20*, 10561–10568.
103. Bui, T. Q.; Bjork, B. J.; Changala, P. B.; Heckl, O. H.; Spaun, B.; Ye, J. OD+CO→D+CO_2 Branching Kinetics Probed with Time-Resolved Frequency Comb Spectroscopy. *Chem. Phys. Lett.* **2017**, *683*, 91–95.
104. Bui, T. Q.; Bjork, B. J.; Changala, P. B.; Nguyen, T. L.; Stanton, J. F.; Okumura, M.; Ye, J. Direct Measurements of DOCO Isomers in the Kinetics of OD + CO. *Sci. Adv.* **2018**, *4*, eaao4777.
105. Bui, T. Q.; Changala, P. B.; Bjork, B. J.; Yu, Q.; Wang, Y.; Stanton, J. F.; Bowman, J.; Ye, J. Spectral Analyses of *trans*- and *cis*-DOCO Transients via Comb Spectroscopy. *Mol. Phys.* **2018**, *116*, 3710–3717.
106. Lins, E.; Read, S.; Unni, B.; Rosendahl, S. M.; Burgess, I. J. Microsecond Resolved Infrared Spectroelectrochemistry Using Dual Frequency Comb IR Lasers. *Anal. Chem.* **2020**, *92*, 6241–6244.
107. Norahan, M. J.; Horvath, R.; Woitzik, N.; Jouy, P.; Eigenmann, F.; Gerwert, K.; Kötting, C. Microsecond-Resolved Infrared Spectroscopy on Nonrepetitive Protein Reactions by Applying Caged Compounds and Quantum Cascade Laser Frequency Combs. *Anal. Chem.* **2021**, *93*, 6779–6783.
108. Fleisher, A. J.; Bjork, B. J.; Bui, T. Q.; Cossel, K. C.; Okumura, M.; Ye, J. Mid-Infrared Time-Resolved Frequency Comb Spectroscopy of Transient Free Radicals. *J. Phys. Chem. Lett.* **2014**, *5*, 2241–2246.
109. Rockmore, R.; Gibson, R.; Moloney, J. V.; Jones, R. J. VECSEL-Based Virtually Imaged Phased Array Spectrometer for Rapid Gas Phase Detection in the Mid-Infrared. *Opt. Lett.* **2020**, *45*, 5796–5799.
110. Luo, P. L.; Horng, E. C. Simultaneous Determination of Transient Free Radicals and Reaction Kinetics by High-Resolution Time-Resolved Dual-Comb Spectroscopy. *Comm. Chem.* **2020**, *3*, 8.
111. Luo, P. L. Long-Wave Mid-Infrared Time-Resolved Dual-Comb Spectroscopy of Short-Lived Intermediates. *Opt. Lett.* **2020**, *45*, 6791–6794.
112. Luo, P. L.; Horng, E. C.; Guan, Y. C. Fast Molecular Fingerprinting with a Coherent, Rapidly Tunable Dual-Comb Spectrometer near 3 mm. *Phys. Chem. Chem. Phys.* **2019**, *21*, 18400–18405.

113. Sterczewski, L. A.; Westberg, J.; Yang, Y.; Burghoff, D.; Reno, J.; Hu, Q.; Wysocki, G. Terahertz Spectroscopy of Gas Mixtures with Dual Quantum Cascade Laser Frequency Combs. *ACS Photonics* **2020**, *7*, 1082–1087.
114. Abbas, M. A.; Pan, Q.; Mandon, J.; Cristescu, S. M.; Harren, F. J. M.; Khodabakhsh, A. Time-Resolved Mid-Infrared Dual-Comb Spectroscopy. *Sci. Rep.* **2019**, *9*, 9.
115. Fjodorow, P.; Allmendinger, P.; Horvath, R.; Herzler, J.; Eigenmann, F.; Geiser, M.; Fikri, M.; Schulz, C. Monitoring Formaldehyde in a Shock Tube with a Fast Dual-Comb Spectrometer Operating in the Spectral Range of 1740-1790 cm^{-1}. *Appl. Phys. B* **2020**, *126*, 11.
116. Hayden, T. R. S.; Malarich, N.; Petrykowski, D.; Nigam, S. P.; Christopher, J. D.; Lapointe, C.; Wimer, N. T.; Hamlington, P. E.; Rieker, G. B. OH Radical Measurements in Combustion Environments using Wavelength Modulation Spectroscopy and Dual-Frequency Comb Spectroscopy Near 1491 nm. *Appl. Phys. B* **2019**, *125*, 14.
117. Pinkowski, N. H.; Cassady, S. J.; Strand, C. L.; Hanson, R. K. Quantum-Cascade-Laser-Based Dual-Comb Thermometry and Speciation at High Temperatures. *Meas. Sci. Technol.* **2021**, *32*, 16.
118. Zhang, G. L.; Horvath, R.; Liu, D. P.; Geiser, M.; Farooq, A. QCL-Based Dual-Comb Spectrometer for Multi-Species Measurements at High Temperatures and High Pressures. *Sensors* **2020**, *20*, 14.
119. Abbas, M. A.; van Dijk, L.; Jahromi, K. E.; Nematollahi, M.; Harren, F. J. M.; Khodabakhsh, A. Broadband Time-Resolved Absorption and Dispersion Spectroscopy of Methane and Ethane in a Plasma Using a Mid-Infrared Dual-Comb Spectrometer. *Sensors* **2020**, *20*, 25.
120. Hoghooghi, N.; Cole, R. K.; Rieker, G. B. 11-ms time-resolved, continuous dual-comb spectroscopy with spectrally filtered mode-locked frequency combs. *Appl. Phys. B* **2021**, *127*, 10.
121. Zhang, Y.; Weeks, R. R. D.; Lecaplain, C.; Harilal, S. S.; Yeak, J.; Phillips, M. C.; Jones, R. J. Burst-Mode Dual-Comb Spectroscopy. *Opt. Lett.* **2021**, *46*, 860–863.
122. Xu, K.; Ma, L. H.; Chen, J.; Zhao, X.; Wang, Q.; Kan, R. F.; Zheng, Z.; Ren, W. Dual-Comb Spectroscopy for Laminar Premixed Flames with a Free-running Fiber Laser. *Combust. Sci. Technol.* **2021**, DOI:10.1080/00102202.2021.1879796.
123. Khan, M. A. H.; Percival, C. J.; Caravan, R. L.; Taatjes, C. A.; Shallcross, D. E. Criegee Intermediates and Their Impacts on the Troposphere. *Environ. Sci.-Process Impacts* **2018**, *20*, 437–453.
124. Welz, O.; Savee, J. D.; Osborn, D. L.; Vasu, S. S.; Percival, C. J.; Shallcross, D. E.; Taatjes, C. A. Direct Kinetic Measurements of Criegee Intermediate (CH_2OO) Formed by Reaction of CH_2I with O_2. *Science* **2012**, *335*, 204–207.
125. Chhantyal-Pun, R.; Khan, M. A. H.; Taatjes, C. A.; Percival, C. J.; Orr-Ewing, A. J.; Shallcross, D. E. Criegee Intermediates: Production, Detection and Reactivity. *Int. Rev. Phys. Chem.* **2020**, *39*, 385–424.
126. Luo, P.-L.; Endo, Y.; Lee, Y.-P. Identification and Self-Reaction Kinetics of Criegee Intermediates *syn*-CH_3CHOO and CH_2OO via High-Resolution Infrared Spectra with a Quantum-Cascade Laser. *J. Phys. Chem. Lett.* **2018**, *9*, 4391–4395.

127. Chang, Y.-P.; Merer, A. J.; Chang, H.-H.; Jhang, L.-J.; Chao, W.; Lin, J. J.-M. High Resolution Quantum Cascade Laser Spectroscopy of the Simplest Criegee Intermediate, CH_2OO, between 1273 cm^{-1} and 1290 cm^{-1}. *J. Chem. Phys.* **2017**, *146*, 244302.
128. Su, Y.-T.; Huang, Y.-H.; Witek, H. A.; Lee, Y.-P. Infrared Absorption Spectrum of the Simplest Criegee Intermediate CH_2OO. *Science* **2013**, *340*, 174–176.
129. Huang, Y.-H.; Li, J.; Guo, H.; Lee, Y.-P. Infrared Spectrum of the Simplest Criegee Intermediate CH_2OO at Resolution 0.25 cm^{-1} and New Assignments of Bands $2n_9$ and n_5. *J. Chem. Phys.* **2015**, *142*, 214301.
130. Gordon, I. E.; Rothman, L. S.; Hill, C.; Kochanov, R. V.; Tan, Y.; Bernath, P. F.; Birk, M.; Boudon, V.; Campargue, A.; Chance, K. V.; Drouin, B. J.; Flaud, J. M.; Gamache, R. R.; Hodges, J. T.; Jacquemart, D.; Perevalov, V. I.; Perrin, A.; Shine, K. P.; Smith, M. A. H.; Tennyson, J.; Toon, G. C.; Tran, H.; Tyuterev, V. G.; Barbe, A.; Császár, A. G.; Devi, V. M.; Furtenbacher, T.; Harrison, J. J.; Hartmann, J. M.; Jolly, A.; Johnson, T. J.; Karman, T.; Kleiner, I.; Kyuberis, A. A.; Loos, J.; Lyulin, O. M.; Massie, S. T.; Mikhailenko, S. N.; Moazzen-Ahmadi, N.; Müller, H. S. P.; Naumenko, O. V.; Nikitin, A. V.; Polyansky, O. L.; Rey, M.; Rotger, M.; Sharpe, S. W.; Sung, K.; Starikova, E.; Tashkun, S. A.; Auwera, J. V.; Wagner, G.; Wilzewski, J.; Wcisło, P.; Yu, S.; Zak, E. J. The HITRAN2016 Molecular Spectroscopic Database. *J. Quant. Spectrosc. Radiat. Transf.* **2017**, *203*, 3–69.
131. Ideguchi, T.; Holzner, S.; Bernhardt, B.; Guelachvili, G.; Picqué, N.; Hänsch, T. W. Coherent Raman Spectro-Imaging with Laser Frequency Combs. *Nature* **2013**, *502*, 355–358.
132. Coluccelli, N.; Howle, C. R.; McEwan, K.; Wang, Y.; Fernandez, T. T.; Gambetta, A.; Laporta, P.; Galzerano, G. Fiber-Format Dual-Comb Coherent Raman Spectrometer. *Opt. Lett.* **2017**, *42*, 4683–4686.
133. Herman, D. I.; Waxman, E. M.; Ycas, G.; Giorgetta, F. R.; Newbury, N. R.; Coddington, I. R. Real-Time Liquid-Phase Organic Reaction Monitoring with Mid-Infrared Attenuated Total Reflectance Dual Frequency Comb Spectroscopy. *J. Mol. Spectrosc.* **2019**, *356*, 39–45.
134. Klocke, J. L.; Mangold, M.; Allmendinger, P.; Hugi, A.; Geiser, M.; Jouy, P.; Faist, J.; Kottke, T. Single-Shot Sub-Microsecond Mid-Infrared Spectroscopy on Protein Reactions with Quantum Cascade Laser Frequency Combs. *Anal. Chem.* **2018**, *90*, 10494–10500.
135. Schnee, J.; Bazin, P.; Barviau, B.; Grisch, F.; Beccard, B. J.; Daturi, M. Coupling a Rapid-Scan FT-IR Spectrometer with Quantum Cascade Lasers within a Single Setup: An Easy Way to Reach Microsecond Time Resolution without Losing Spectral Information. *Anal. Chem.* **2019**, *91*, 4368–4373.
136. Qin, Y.; Cromey, B.; Batjargal, O.; Kieu, K. All-Fiber Single-Cavity Dual-Comb for Coherent Anti-Stokes Raman Scattering Spectroscopy Based on Spectral Focusing. *Opt. Lett.* **2021**, *46*, 146–149.
137. Kameyama, R.; Takizawa, S.; Hiramatsu, K.; Goda, K. Dual-Comb Coherent Raman Spectroscopy with near 100% Duty Cycle. *ACS Photonics* **2020**, *8*, 975.
138. Han, N. S.; Kim, J.; Yoon, T. H.; Cho, M. Broadband Infrared Spectroscopy of Molecules in Solutions with Two Intrapulse Difference-Frequency-Generated Mid-Infrared Frequency Combs. *J. Phys. Chem. B* **2021**, *125*, 307–316.
139. Cho, Y. E.; Maeng, J. Y.; Kim, S.; Hong, S. Formation of Highly Ordered Organic Monolayers by Dative Bonding: Pyridine on Ge(100). *J. Am. Chem. Soc.* **2003**, *125*, 7514–7515.

140. Wolkow, R. A. Controlled Molecular Adsorption On Silicon: Laying a Foundation for Molecular Devices. *Annu. Rev. Phys. Chem.* **1999**, *50*, 413–441.
141. Waxman, E. M.; Cossel, K. C.; Truong, G. W.; Giorgetta, F. R.; Swann, W. C.; Coburn, S.; Wright, R. J.; Rieker, G. B.; Coddington, I.; Newbury, N. R. Intercomparison of Open-Path Trace Gas Measurements with Two Dual-Frequency-Comb Spectrometers. *Atmos. Meas. Tech.* **2017**, *10*, 3295–3311.
142. Ycas, G.; Giorgetta, F. R.; Cossel, K. C.; Waxman, E. M.; Baumann, E.; Newbury, N. R.; Coddington, I. Mid-Infrared Dual-Comb Spectroscopy of Volatile Organic Compounds Across Long Open-Air Paths. *Optica* **2019**, *6*, 165–168.
143. Ycas, G.; Giorgetta, F. R.; Friedlein, J. T.; Herman, D.; Cossel, K. C.; Baumann, E.; Newbury, N. R.; Coddington, I. Compact Mid-Infrared Dual-Comb Spectrometer for Outdoor Spectroscopy. *Opt. Express* **2020**, *28*, 14740–14752.
144. Alden, C. B.; Wright, R. J.; Coburn, S. C.; Caputi, D.; Wendland, G.; Rybchuk, A.; Conley, S.; Faloona, I.; Rieker, G. B. Temporal Variability of Emissions Revealed by Continuous, Long-Term Monitoring of an Underground Natural Gas Storage Facility. *Environ. Sci. Technol.* **2020**, *54*, 14589–14597.
145. Makowiecki, A. S.; Steinbrenner, J. E.; Wimer, N. T.; Glusman, J. F.; Lapointe, C. B.; Daily, J. W.; Hamlington, P. E.; Rieker, G. B. Dual Frequency Comb Spectroscopy of Solid Fuel Pyrolysis and Combustion: Quantifying the Influence of Moisture Content in Douglas Fir. *Fire Saf. J.* **2020**, *116*, 8.
146. Schliesser, A.; Brehm, M.; Keilmann, F.; van der Weide, D. W. Frequency-Comb Infrared Spectrometer for Rapid, Remote Chemical Sensing. *Opt. Express* **2005**, *13*, 9029–9038.
147. Truong, G.-W.; Waxman, E. M.; Cossel, K. C.; Baumann, E.; Klose, A.; Giorgetta, F. R.; Swann, W. C.; Newbury, N. R.; Coddington, I. Accurate Frequency Referencing for Fieldable Dual-Comb Spectroscopy. *Opt. Express* **2016**, *24*, 30495–30504.
148. Cossel, K. C.; Waxman, E. M.; Giorgetta, F. R.; Cermak, M.; Coddington, I. R.; Hesselius, D.; Ruben, S.; Swann, W. C.; Truong, G.-W.; Rieker, G. B.; Newbury, N. R. Open-Path Dual-Comb Spectroscopy to an Airborne Retroreflector. *Optica* **2017**, *4*, 724–728.
149. Rieker, G. B.; Giorgetta, F. R.; Swann, W. C.; Kofler, J.; Zolot, A. M.; Sinclair, L. C.; Baumann, E.; Cromer, C.; Petron, G.; Sweeney, C.; Tans, P. P.; Coddington, I.; Newbury, N. R. Frequency-Comb-Based Remote Sensing of Greenhouse Gases over Kilometer Air Paths. *Optica* **2014**, *1*, 290–298.
150. Yang, K.; Li, H.; Gong, H.; Shen, X.; Hao, Q.; Yan, M.; Huang, K.; Zeng, H. Temperature Measurement Based on Adaptive Dual-Comb Absorption Spectral Detection. *Chin. Opt. Lett.* **2020**, *18*, 051401.
151. Waxman, E. M.; Cossel, K. C.; Giorgetta, F.; Truong, G. W.; Swann, W. C.; Coddington, I.; Newbury, N. R. Estimating Vehicle Carbon Dioxide Emissions from Boulder, Colorado, Using Horizontal Path-Integrated Column Measurements. *Atmos. Chem. Phys.* **2019**, *19*, 4177–4192.
152. Shimizu, Y.; Okubo, S.; Onae, A.; Yamada, K. M. T.; Inaba, H. T. Molecular Gas Thermometry on Acetylene using Dual-Comb Spectroscopy: Analysis of Rotational Energy Distribution. *Appl. Phys. B* **2018**, *124*, 8.

153. Coburn, S.; Alden, C. B.; Wright, R.; Cossel, K.; Baumann, E.; Truong, G. W.; Giorgetta, F.; Sweeney, C.; Newbury, N. R.; Prasad, K.; Coddington, I.; Rieker, G. B. Regional Trace-Gas Source Attribution Using a Field-Deployed Dual Frequency Comb Spectrometer. *Optica* **2018**, *5*, 320–327.
154. Wang, C.; Sahay, P. Breath Analysis Using Laser Spectroscopic Techniques: Breath Biomarkers, Spectral Fingerprints, and Detection Limits. *Sensors* **2009**, *9*, 8230–8262.
155. Metsala, M. Optical Techniques for Breath Analysis: From Single to Multi-Species Detection. *J. Breath. Res.* **2018**, *12*, 027104.
156. Li, J. Y.; Yu, Z. W.; Du, Z. H.; Ji, Y.; Liu, C. Standoff Chemical Detection Using Laser Absorption Spectroscopy: A Review. *Remote Sens.* **2020**, *12*, 44.
157. Spinelle, L.; Gerboles, M.; Kok, G.; Persijn, S.; Sauerwald, T. Review of Portable and Low-Cost Sensors for the Ambient Air Monitoring of Benzene and Other Volatile Organic Compounds. *Sensors* **2017**, *17*, 30.
158. Abreu, P.; Carslaw, D.; Davies, T.; Dernie, J.; Kent, A.; Stacey, B.; Telling, S.; Wakeling, D. *UK Hydrocarbons Network Annual Report for 2015*; Defra (Department for the Environment Food and Rural Affairs), Ricardo-AEA, 2016.
159. Chen, T.; Xue, L.; Zheng, P.; Zhang, Y.; Liu, Y.; Sun, J.; Han, G.; Li, H.; Zhang, X.; Li, Y.; Li, H.; Dong, C.; Xu, F.; Zhang, Q.; Wang, W. Volatile Organic Compounds and Ozone Air Pollution in an Oil Production Region in Northern China. *Atmos. Chem. Phys.* **2020**, *20*, 7069–7086.
160. Li, S.-M.; Leithead, A.; Moussa, S. G.; Liggio, J.; Moran, M. D.; Wang, D.; Hayden, K.; Darlington, A.; Gordon, M.; Staebler, R.; Makar, P. A.; Stroud, C. A.; McLaren, R.; Liu, P. S. K.; O'Brien, J.; Mittermeier, R. L.; Zhang, J.; Marson, G.; Cober, S. G.; Wolde, M.; Wentzell, J. J. B. Differences Between Measured and Reported Volatile Organic Compound Emissions from Oil Sands Facilities in Alberta, Canada. *Proc. Natl. Acad. Sci. USA* **2017**, 201617862.
161. Cooke, I. R.; Sims, I. R. Experimental Studies of Gas-Phase Reactivity in Relation to Complex Organic Molecules in Star-Forming Regions. *ACS Earth Space Chem.* **2019**, *3*, 1109–1134.
162. Yue, J.; Schouten, J. C.; Nijhuis, T. A. Integration of Microreactors with Spectroscopic Detection for Online Reaction Monitoring and Catalyst Characterization. *Ind. Eng. Chem. Res.* **2012**, *51*, 14583–14609.
163. Pereira, J.; Porto-Figueira, P.; Cavaco, C.; Taunk, K.; Rapole, S.; Dhakne, R.; Nagarajaram, H.; Câmara, J. S. Breath Analysis as a Potential and Non-Invasive Frontier in Disease Diagnosis: An Overview. *Metabolites* **2015**, *5*, 3–55.